AD-A096 947 CERAMIC FINISHING CO STATE COLLEGE PA F/G 11/2
LOCALIZED IMPACT DAMAGE IN CERAMICS: COMPARISONS OF RECENT EXPE--ETC(U)
JUL 80 H P KIRCHNER, T J LARCHUK N00014-74-C-0241
UNCLASSIFIED NL

1 OF 1
AD A 096947

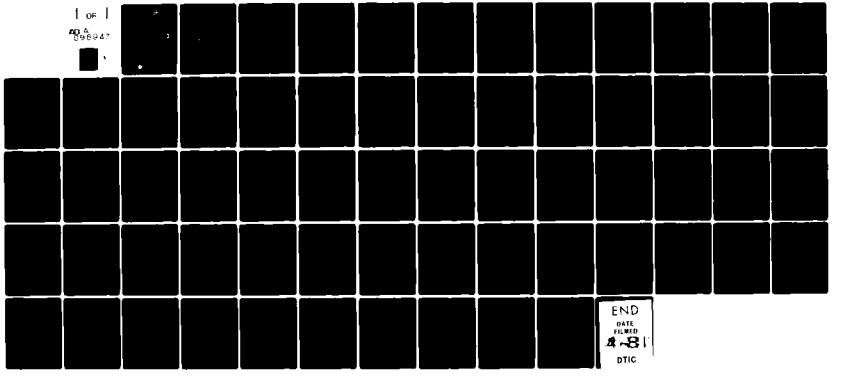

END
DATE FILMED
4-81
DTIC

LEVEL II

1

6/

LOCALIZED IMPACT DAMAGE IN CERAMICS:

COMPARISONS OF RECENT EXPERIMENTS AND THEORETICAL CALCULATIONS

11 Jul[redacted]80

12

Prepared by
10 H. P. Kirchner
T. J. Larchuk

15

Prepared under Contract No. N00014-74-C-0241
for the Office of Naval Research, Department of the Navy
Requisition No. NR032-545/12-17-73 (471)

CERAMIC FINISHING COMPANY
P. O. Box 498, State College, Pa. 16801

TABLE OF CONTENTS

I. Introduction

The objective of the present investigation is to make a comprehensive experimental evaluation of a recent theory of elastic-plastic impact[2] and to modify the theory to provide a more realistic description of the impact characteristics. Previous work has included investigation of subsonic localized impact damage in glass[2,7], ZnS[1,8,9], transformation toughened zirconia (TT-$2rO_2$)[1,10,11], and other ceramics[12,14]. A major advantage of the theory is that it provides a means to predict the response of a material subjected to impact loading using contact characteristics determined by static loading tests. The assumption that the damage induced at a particular maximum static load is the same as that resulting from an equal maximum impact load has frequently been invoked or suggested[15,16]. A recent report describes similarities and differences in damage induced by static and impact loading[8]. A preliminary evaluation of the theory of elastic-plastic impact using limited data showed that the theory yields promising results[17]. The present report describes certain modifications of the theory and a more complete evaluation of the theory based on more extensive data.

II. Experimental Procedures

Glass, CVD ZnS, and TT-ZrO_2 plates described in Table I were prepared as follows:

Glass--Larger glass plates were cut using a glass cutter to form the square specimens.

ZnS--The square plates were used in the polished condition in which they were secured from the manufacturer.

TT-ZrO_2--The calcia partially stabilized zirconia plates were prepared at CSIRO where they were aged at 1300°C for various periods of time to form three grades in which the K_{IC} increased with increasing aging time (as fired, 0 hours; under aged, 30 hours; peak aged, 48 hours). At Ceramic Finishing Company the TT-ZrO_2 plates were polished on one surface using 1/4 μm diamond powder as the last step. These specimens were fractured in earlier experiments and the remaining ends of these specimens were used in the present experiments.

The physical properties of the materials are listed in Table II.

The plates were coated with a thin layer of soot by moving the plates back and forth through a candle flame until a layer of sufficient thickness was formed. The imprint of the sphere in the soot layer was used to measure the contact radius. The assumption that the radius of the imprint represents the contact radius, including the effects of variation in soot layer thickness, is discussed in a later section.

Table I. Description of Specimens.

Plates			Spheres		
Material	Specimen Dimensions mm	Source	Material	Specimen Dimensions mm	Source
Soda-lime-glass	5 x 30 x 30	Centre Glass State College, PA	Glass	3.0	Walter Stern, Inc. Port Washington, NY
CVD ZnS	7 x 26 x 26	Raytheon Company Waltham, MA	Glass	3.0	Same as above
TT-ZrO_2*	4 x 11 x 32	CSIRO Melbourne, Australia	Tungsten Carbide Grade 25	1.59	Ultraspherics, Inc. Sault St. Marie MI

*Three grades of TT-ZrO_2 were provided by R. C. Garvie of CSIRO.

Table II. Material Properties.

Property	Material			
	Glass	ZnS	TT-ZrO_2	Tungsten Carbide
Young's Modulus MPa	68,000[i]	74,100[a]	11,000[f]	410,000[c] 650,000
Poisson's Ratio	***	0.30[a] (in plane of plate)	**	**
Density Kgm^{-3}	2,500*	4,090[a]	0	15,000[c]
Critical Stress Intensity Factor $MPam^{1/2}$	0.7	1[d] 0.75[h] 0.67[a]	As fired 4.5[g] Under Aged 5.6 Peak Aged 6.5	---
Hardness GPa	5.3[e]	1.9[d]	12.9 $\pm$ .78[b]	---
Average Grain Size µm	---	30[d]	As fired 67 $\pm$ 7[f] Under Aged 70 $\pm$ 21 Peak Aged 79 $\pm$ 24	

* Calculated from measured diameter and mass.
** Assumed to be 0.3 for calculations involving equations for the elastic case (see Table III).
*** Assumed to be 0.24 for calculations involving equations for the elastic case (see Table III).

(a) W. F. Adler, T. W. James, "Localized Deformation and Fracture of Transparent Ceramics," Effects Technology, Inc., Technical Report, March 1980, ONR contract N00014-76-C-0744 NR 032-565.

(b) R. C. Garvie, R. R. Hughan, and R. T. Pascoe, "Strengthening of Lime-Stabilized Zirconia by Post Sintering Heat Treatments," from "Processing of Crystalline Ceramics," Hayne Palmour III, R. F. Davis, and T. M. Hare, editors, Plenum Publishing Corp. (1978).

(c) N. P. Suh and A. P. L. Turner, "Elements of the Mechanical Behavior of Solids," McGraw-Hill (1975).

(d) A. G. Evans and T. R. Wilshaw, "Quasi-Static Solid Particle Damage in Brittle Solids, I, Observations, Analyses, and Implications," Acta. Met. 24, 939-956 (1976).

(e) R. W. Rice, "Correlation of Hardness with Mechanical Effects in Ceramics," from The Science of Hardness Testing and Its Research Applications, Edited by J. H. Westbrook and H. Conrad, American Society for Metals (1973), p. 117-133.

(f) R. C. Garvie, R. H. J. Hannink and C. Urbani, "Fracture Mechanics Study of a Transformation Toughened Zirconia Alloy in the CaO-ZrO_2 System," Presented at 4th CIMTEC Meeting, Saint-Vincent, Italy (May, 1979).

(g) H. P. Kirchner, R. M. Gruver, M. V. Swain, R. C. Garvie, "Crack Propagation and Branching in Transformation Toughened Zirconia," Submitted for publication.

(h) D. A. Shockey, D. J. Rowcliffe, and K. C. Dao, "Fracture Toughness of CVD ZnS," Stanford Research Institute Topical Report, Contract N00014-76-C-0657 (March 1977).

(i) J. Congleton and N. J. Petch, "Crack-Branching," Phil. Mag. Series 8, Vol. 16, 749-760 (1967).

The specimens were subjected to either static or impact loading. The static loads were applied using a table top, Instron testing machine. When the glass spheres were used as indenters, the spheres were fastened to the crosshead and the glass or ZnS plates were placed on the load cell. The tungsten carbide spheres were fastened to the load cell and the TT-ZrO_2 specimens were fastened to the cross head because of problems involved in gluing the very small spheres to the cross head.

For impact loading, the spheres were coated with a thin layer of aluminum to improve their reflectivity and accelerated using a gas gun with compressed N_2 gas. The specimens were mounted on a steel plate with a large surface perpendicular to the path of the sphere. The impacting and rebounding velocities of the spheres were measured using photographs taken using a camera with anopen shutter. The spheres were illuminated at known time intervals using a stroboscope and the velocities were calculated by dividing the distance between images by the time interval.

The contact and indentation radii were measured using a grid in the eyepiece of a microscope.

III. Review of the Theory

The theory of elastic-plastic impact[1] is based on the following empirical relations for static loading:

$$\eta = \kappa(r_c/r_o)^{\xi} \tag{1}$$

$$\eta' = \kappa'(r_i/r_o)^{\xi'} \tag{2}$$

where η and η' are the contact and indentation pressures, respectively; r_c is the contact radius, r_i is the indentation radius, and κ, κ', ξ and ξ' are contact characteristics that are determined from log-log plots of η vs r_c/r_o and η' vs r_i/r_o.

The characteristics ξ and ξ' account for work hardening and other material characteristics that control the deformation under static loading conditions. The characteristic κ represents the pressure at which the contact radius equals the radius of the spherical indenter. Likewise, κ' represents the pressure at which the indentation radius equals the radius of the spherical intenter. At high r/r_o ratios, Equations (1) and (2) no longer apply because of deformation of the sphere and increasing errors in the geometrical assumptions. Also, for a given material we would expect κ to be less than κ', because r_i is less than r_c for all $r < r_o$ so that the indentation area is less than the contact area and η is less than η'.

The pressures are taken to be the load divided by the projection of the area, so that (1) and (2) can also be written in the form

$$P = \pi \kappa r_o^2 (r_c/r_o)^{\xi+2} \tag{3}$$

$$P = \pi \kappa' r_o^2 (r_i/r_o)^{\xi'+2} \tag{4}$$

An expression for the impact loading contact radius can be derived by assuming that the sphere remains rigid. Then, the work done by the load as given in Equation (3), to the point of maximum penetration, can be equated to the initial kinetic energy of the impacting sphere. This yields*

$$r_c = r_o \left[\frac{M(\xi+4)}{2\kappa\pi r_o^3}\right]^{\frac{1}{\xi+4}} V_o^{\frac{2}{\xi+4}} \tag{5}$$

By assuming that equal static and impact loads result in equal contact radii we can substitute for r_c in Equation (3) using Equation (5) to get the following expression for the impact load

$$P = \kappa \pi r_o^2 \left[\frac{M(\xi+4)}{2\kappa\pi r_o^3}\right]^{\frac{\xi+2}{\xi+4}} V_o^{\frac{2(\xi+2)}{(\xi+4)}} \tag{6}$$

*This method neglects the stress wave energy and the fracture surface energy.

Similar manipulations provide expressions for the indentation radius, penetration time, depth of damage, remaining strength, contact time, and coefficient of restitution. The equations used in the present work are given in Table III which also includes equations for completely elastic response which will be referred to as the Hertzian case[17,27].

Modification of the Analyses

Roesler and others[18,19] used dimensional analysis and energy arguments to derive equations describing the variation of crack size (c) due to varying contact load (P) in the "far field" where the effects of the nature of the particular contact are considered to be small. In the form used by Lawn and Marshall[20] this equation is

$$P = \frac{K_{Ic}}{\chi} c^{3/2} \tag{7}$$

in which K_{Ic} is the critical stress intensity factor and χ is a constant that accounts for geometrical and frictional characteristics of the contact. The equation was incorporated into the original analysis of elastic-plastic impact to permit calculation of the depth of damage and the remaining strength. However, in an investigation of penetration of damage during single point diamond grinding of ceramics, Kirchner, Gruver, and Richard[21] found that for diamond points with varying sharpness, the depth of damage (c) varied systematically with the length of contact even in the "far field" where the effect of contact characteristics was expected to be minimal.

Table III. Equations for Impact Characteristics*.

Characteristic	Hertzian (Elastic) Theory[17,27]	Elastic-Plastic Impact Theory[1]
Contact Radius	$r_o = [\frac{4Qr_o P}{3E_2}]^{1/3}$	$r_c = r_o[\frac{M(\xi+4)}{2\kappa\pi r_o^3}]^{\frac{1}{\xi+4}} V_o^{\frac{2}{\xi+4}}$
Indentation Radius	No Indentation	$r_i = r_o[(\frac{\kappa}{\kappa'})(\frac{M(\xi+4)}{2\kappa\pi r_o^3})^{\frac{\xi+2}{\xi+4}}]^{\frac{1}{\xi'+2}} V_o^{\frac{2(\xi+2)}{(\xi+4)(\xi'+2)}}$
Impact Load	$P = 1.14\{[\frac{16}{9\pi^2}][\frac{M^3 V_o^6 r_o}{(K_i+K_2)^2}]\}^{1/5}$	$P = \Omega V_o^{\frac{2(\xi+2)}{\xi+4}}$, $\Omega = \kappa\pi r_o^2 [\frac{M(\xi+4)}{2\kappa\pi r_o^3}]^{\frac{\xi+2}{\xi+4}}$
Coefficient of Restitution	$e = 1$	$e = \{1-[(\frac{\kappa}{\kappa'})(\frac{M(\xi+4)}{2\kappa\pi r_o^3})^{\frac{\xi+4}{\xi'+2}} V_o^{\frac{\xi-\xi'}{\xi'+2}}]^{\frac{2(\xi-\xi')}{\xi'+2}}\}^{1/2}$
Depth of Damage		$c^{1/2} = \frac{1}{\beta}[(P/d_i)_{impact} - \alpha]$ where, $(P/d_i)_{impact} = P/2r_i$ from above equations.

*See list of symbols on following page.

List of Symbols

η - Contact pressure

η' - Indentation pressure

κ - Resistance to Penetration

κ' - Resistance to indentation

κ_m - Modified κ

ξ - Exponent characteristic of the variation of the contact pressure with increasing load

ξ' - Exponent related to work hardneing

ξ_m - Modified ξ

r_o - Radius of impacting sphere

M - Mass of impacting sphere

r_c - Contact radius

r_i - Indentation radius

P - Maximum load perpendicular to the surface

E_j - Young's modulus $j = 1$ for sphere, $j = 2$ for plate

U_i - Poisson's ratio $j = 1, 2$ as above

Q - $Q = \frac{9}{16}[(1-\nu_2^2) + (1-\nu_1^2)\frac{E_2}{E_1}$

V_o - Impact velocity

K_j - $K_j = \frac{(1-\nu_i)}{\pi E_j}$

e - Coefficient of restitution

Ω - $\Omega = \kappa\pi r_o^2 [\frac{M(\xi+4)}{2\kappa\pi r_o}]^{\frac{\xi+2}{\xi+4}}$

d_i - Indentation diameter

c - Crack length

α, β - Constants determined from static data where $P/d_i = \alpha + \beta c^{1/2}$

K_{Ic} - *Critical stress intensity factor*

χ - Proportionality factor accounting for unknown geometrical and frictional factors

z_o - Depth of the disturbed zone

Based on the above observations, Conway and Kirchner[22] analyzed penetration of surface damage for the case in which a "disturbed" zone is formed under the contact. This "disturbed" zone may be formed as a result of plastic deformation, shear cracking or crushing under the contact. This analysis yielded a relation of the form

$$P \propto z_o c^{1/2} \tag{8}$$

in which z_o is the depth of the disturbed zone. A proportionality factor can be introduced which accounts for other characteristics of the contact and variations in K_{Ic} from one material to another. Similar relations might arise as a result of line contact loading, wedging, or residual stresses.

Shear failures under contacts have characteristic flow or crack patterns that follow shear stress trajectories[23]. Based on the shapes of these patterns there appears to be a direct relationship between the depth of the disturbed zone and the contact width. Therefore, it may be appropriate in many cases, such as single point diamond grinding with diamonds having various degrees of sharpness, to substitute the contact width for z_o in the above relation.

A "disturbed" zone has been observed in ZnS statically indented by glass spheres. When the indentation diameter (d_i) was substituted for z_o in the above relation and P/d_i was plotted vs $c^{1/2}$ a good linear fit was observed[8,9].

Based on the above experience, relation (8) has been substituted for Equation (7) in the original derivations of the equations for calculating the depth of damage and the remaining strength after impact.

Remedies for a Problem in Measuring r_c

As mentioned previously, one should expect κ to be less than κ' because $r_c > r_i$ in all cases. However, experimentally one finds that, as shown in Figure 1, the extension of the data representing the contact tends to intersect the data representing the indentation at a point $r < r_o$ rather than at $r = r_o$. Two possible explanations of the observation were considered:

1. The elastic recovery in the plane of the specimen surface may decrease r_c substantially[28].

2. The increased discontinuity at the rim of the indentation with increasing indentation size may cause r_c to increase less with load than otherwise expected. In terms of the graph this implies a shallower slope than the original contact radius curve and an intersection at $r \leq r_c$.

It is unfortunate that the cause of the difficulty is not understood because the remedies implied by the above explanations are quite different. In the first case it is reasonable to assume, because the yield stress is exceeded, that the correct curve is simply shifted to the right as indicated in Figure 2, so that it intersects at $r = r_o$. This is the same as substituting κ' for κ. In the second case the data at low r_c/r_o would be considered to be relatively good but the errors would become greater at higher values

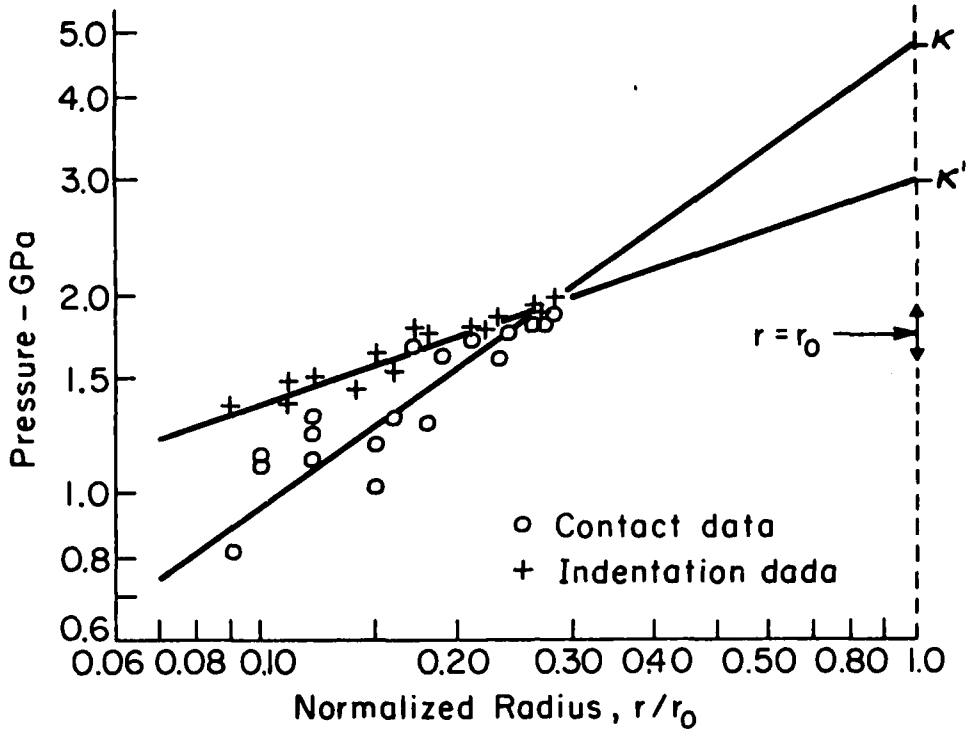

Figure 1 Contact pressure vs. normalized contact radius and indentation pressure vs. normalized indentation radius (ZnS, 3 mm diameter glass spheres).

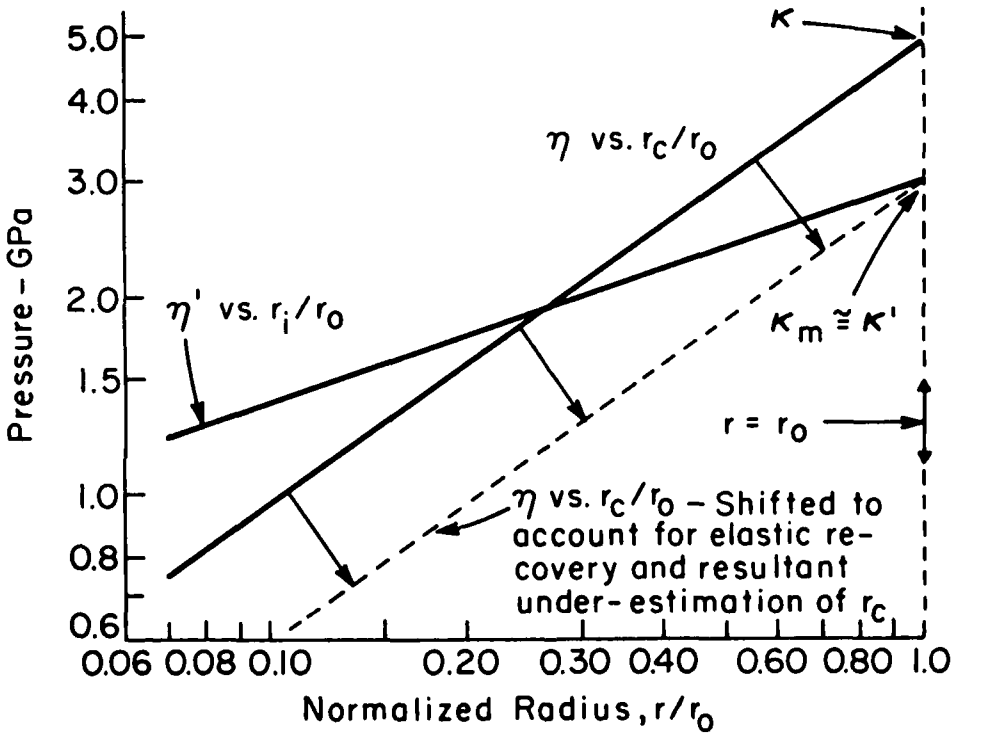

Figure 2 Relative position of the η vs. r_c/r_o curve to the η' vs. r_i/r_o curve and the shift in the η vs. r_i/r_o curve which might be necessary if r_c has been underestimated due to elastic recovery. For ZnS (3 mm diameter glass spheres), but typical of other materials tested.

of r_c/r_o. Therefore, in this case it is reasonable to connect the good data points at low r_o/r_o values with $r_c = r_o$ as shown in Figure 3.

In any event it was decided to assume that $\kappa = \kappa'$ and to refer to this case as the modified elastic-plastic theory. One would expect that if the other choice had been made the results would have fallen, in most cases, between those of the original and modified theories.

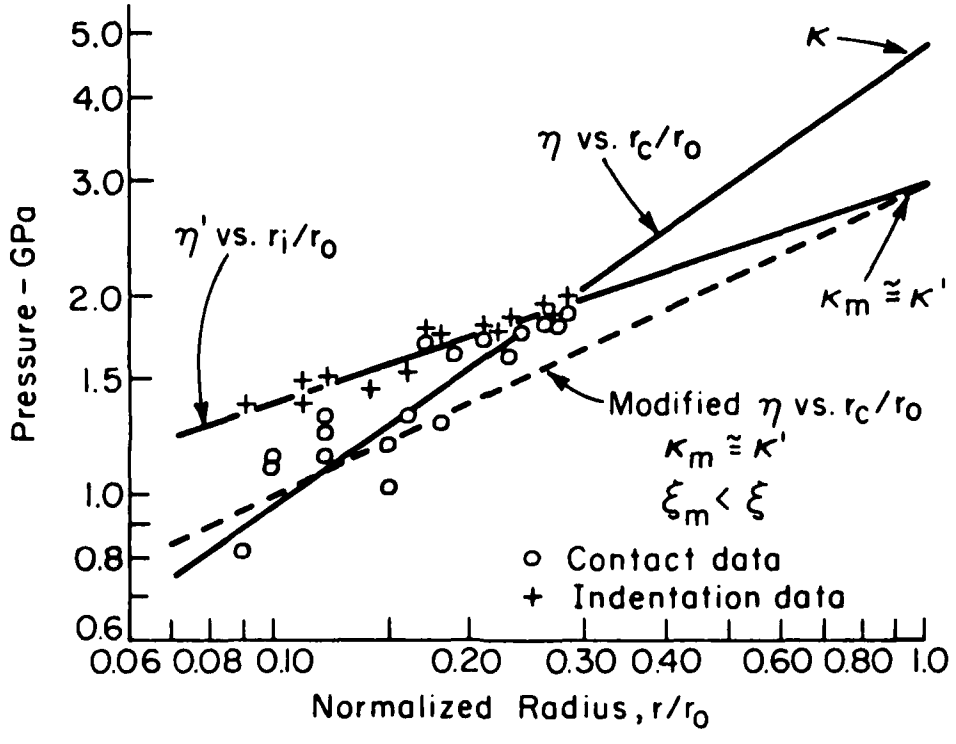

[illegible] η' vs. r_i/r_o curve, η vs. r_c/r_o curve, and a modified η vs. r_c/r_o curve which assumes that increasing discontinuities at increasing indentation radii cause a lower than expected contact radius.

IV. Determination of κ, κ', ξ, and ξ'

In the case of the statically loaded specimens, η and η' were determined by dividing the applied load by the contact area and the indentation area, respectively. Then, η was plotted vs (r_c/r_o) and η' was plotted vs r_i/r_o on log-log plots as suggested by equations (1) and (2). κ, κ', ξ, and ξ' were calculated from the slopes of these plots (Table IV).

The original data were less accurate than desired. The principal problem involved measurement of the contact radius. The soot layer which is used to measure r_c must be thick enough to provide a distinct contrast at the edge of the impression so that an accurate measurement can be made, but, if the soot layer is too thick, the sphere will pick up soot from outside the contact area. In some cases this results in an irregular boundary. The minimum radii were measured in these cases. Because the soot layer was applied manually the thickness varied to some extent from specimen to specimen. The data points representing cases in which the soot layer is definitely too thick are noted on some of the graphs. In general, the r_i measurements are more accurate and less scattered than the r_c measurements. One benefit of substituting κ' for κ as is done in the modified theory is that it suppresses some of the effect of inaccuracies in the r_c measurements.

Table IV. Statically Determined Contact Characteristics for Several Sphere-Plate Combinations.

Materials		Sphere Diameter mm	Static Contact Characteristics			
Plate	Sphere		ξ	κ-GPa	ξ'	κ'-GPa
Glass[a]	Glass	3.0×10^{-3}	2.20[a]	125.6[a]	---	---
Glass[c]	Glass	3.0×10^{-3}	2.04[c]	46.9[c]	---	---
ZnS[b]	Glass	3.0×10^{-3}	0.71[b]	4.9[b]	0.34[b]	3.0[b]
ZnS[c]	Glass	3.0×10^{-3}	0.78[c]	5.5[c]	0.27[c]	5.5[c]
TT ZrO_2[a] As fired	WC	1.59×10^{-3}	0.85[a]	36.6[a]	0.47[a]	21.9[a]
TT ZrO_2[c] As fired	WC	1.59×10^{-3}	1.06[c]	28.5[c]	0.52[c]	22.0[c]
TT ZrO_2[a] Polished 1	WC	1.59×10^{-3}	0.76[a]	30.1[a]	0.51[a]	23.0[a]
TT ZrO_2[a] Polished	WC	1.59×10^{-3}	0.74[a]	29.0[a]	0.53[a]	23.3[a]

[a] New values.
[b] ONR Contract No. N00014-74-0241 Technical Report Number 8, February, 1980.
[c] ONR Contract No. N00014-74-0241 Technical Report Number 7, January, 1979.

V. Experimental Evaluation of the Elastic-Plastic Impact Theory

Glass Spheres on Glass Plates

This material combination involving glass spheres and glass plates represents an end member case in which the response at low impact velocities is almost completely elastic. Therefore, one would expect the Hertzian elasticity theory to provide a good description of the impact. The contact characteristics were $\xi = 2.2$ and $\kappa = 126$ GPa. The glass does not indent permanently so ξ' and κ' were not determined.

The contact radii predicted for various impact velocities are compared with the Hertzian theory predictions in Figure 4. The Hertzian theory fits the data best as expected but both theories yield reasonable approximations. At the highest impact velocities above 100 ms^{-1} crushing occurred, increasing the contact radii above the values otherwise expected. At intermediate velocities ring and cone cracks formed in many specimens. There is no definite evidence that the presence of these cracks affected the contact radii.

The loads predicted for various impact velocities are plotted in Figure 5. The predictions of the two theories agree at low velocities but at higher velocities the elastic-plastic prediction leads to higher loads than the Hertzian theory. Again, because the response of the glass is elastic, one would expect the Hertzian theory to yield the best results.

The impact indentation radii and coefficients of restitution were not calculated for impacts of glass spheres on glass plates because the absence of indentation prevented determination of κ' and ξ'.

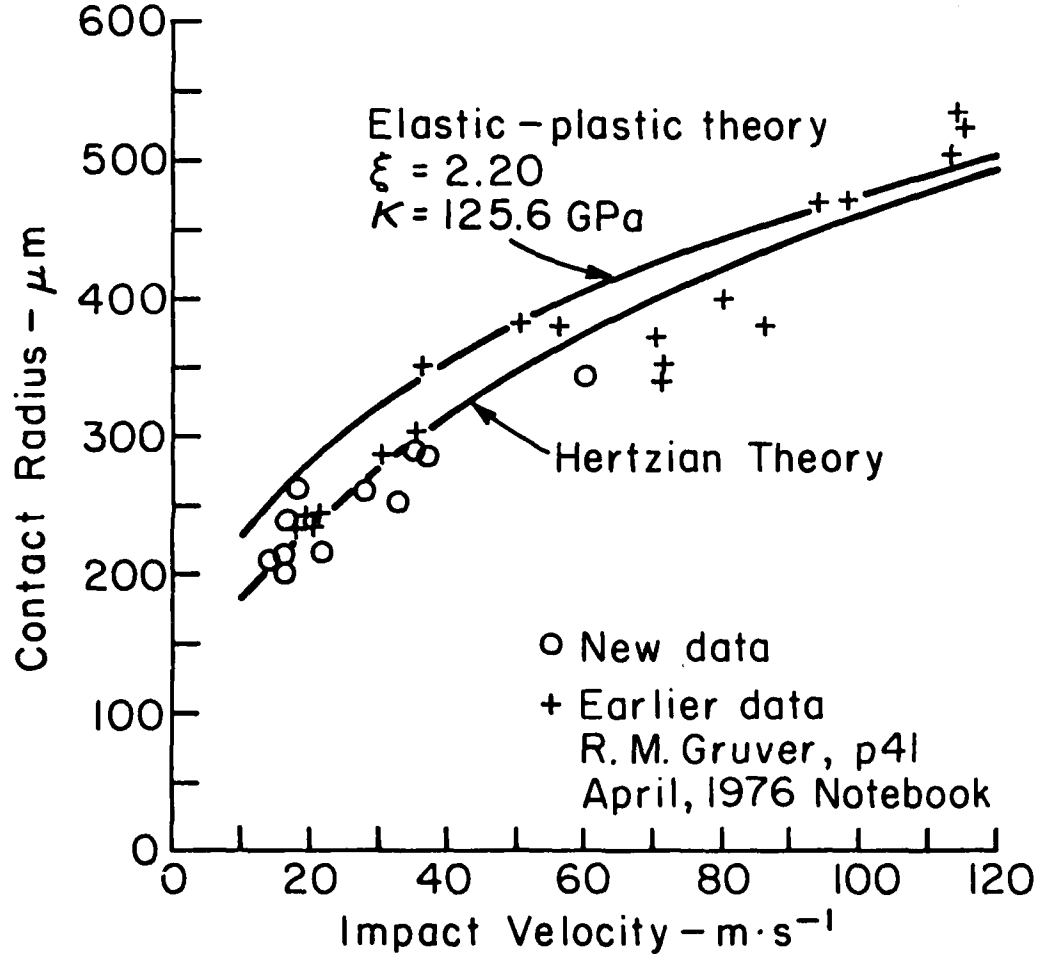

Figure 4. Comparison of theoretical impact contact radii for elastic-plastic and elasticity (Hertzian) theories (glass plates, 3 mm diameter glass spheres).

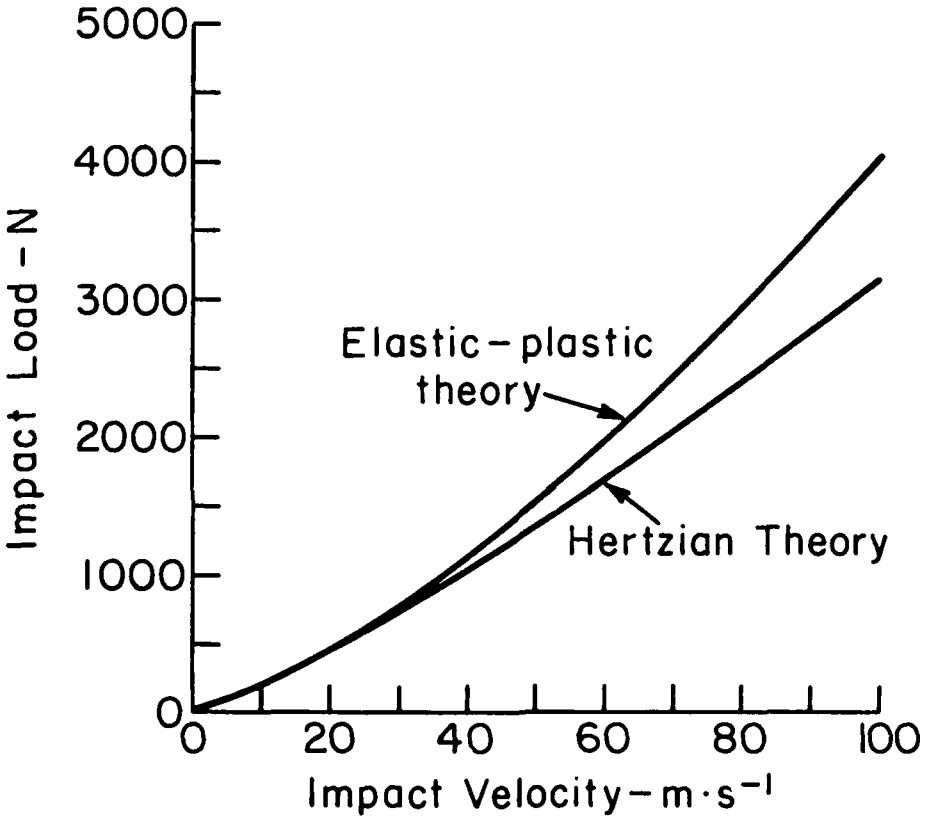

Figure 5 Comparison of theoretical impact loads for elastic-plastic and Hertzian theories. (glass plates, 3 mm diam. x r glass spheres).

Glass Spheres on ZnS Plates

In contrast to the case of glass on glass, impacts of the glass spheres on the ZnS plates yield an elastic-plastic response. Under static loading conditions, indentations were first observed at a 40 N load but a load of 72 N was necessary to obtain a measurable indentation. Indentations were observed at all impact sites. Impact velocities less than about 19 ms^{-1} were impractical because the curvature of the trajectory made it difficult to hit the target.

The static contact characteristics are given in Table IV. The recently reported values which were $\xi = 0.71$, $\kappa = 4.9$ GPa, $\xi' = 0.34$, and $\kappa' = 3.0$ GPa were used to calculate various predicted curves which are compared with the Hertzian theory and experimental results. In some cases κ was assumed to be equal to κ' as described in Section III. These results are called the modified elastic-plastic theory results.

The contact radius results plotted in Figure 6 show that the contact radii are only slightly larger than the Hertz theory predictions and substantially less than the other predictions. There are several factors contributing to errors in these predictions including the strain rate dependence of the flow stress, neglect of the stress wave energy, neglect of the fracture energy, and so forth. The above data supports our earlier conclusion that the most important source of error is the strain rate dependence of the flow stress[8]. As the strain rate increases, the flow stress increases and the material responds more elastically than it does under the static loading conditions used to determine the contact characteristics. This more elastic response shifts the results toward the Hertzian

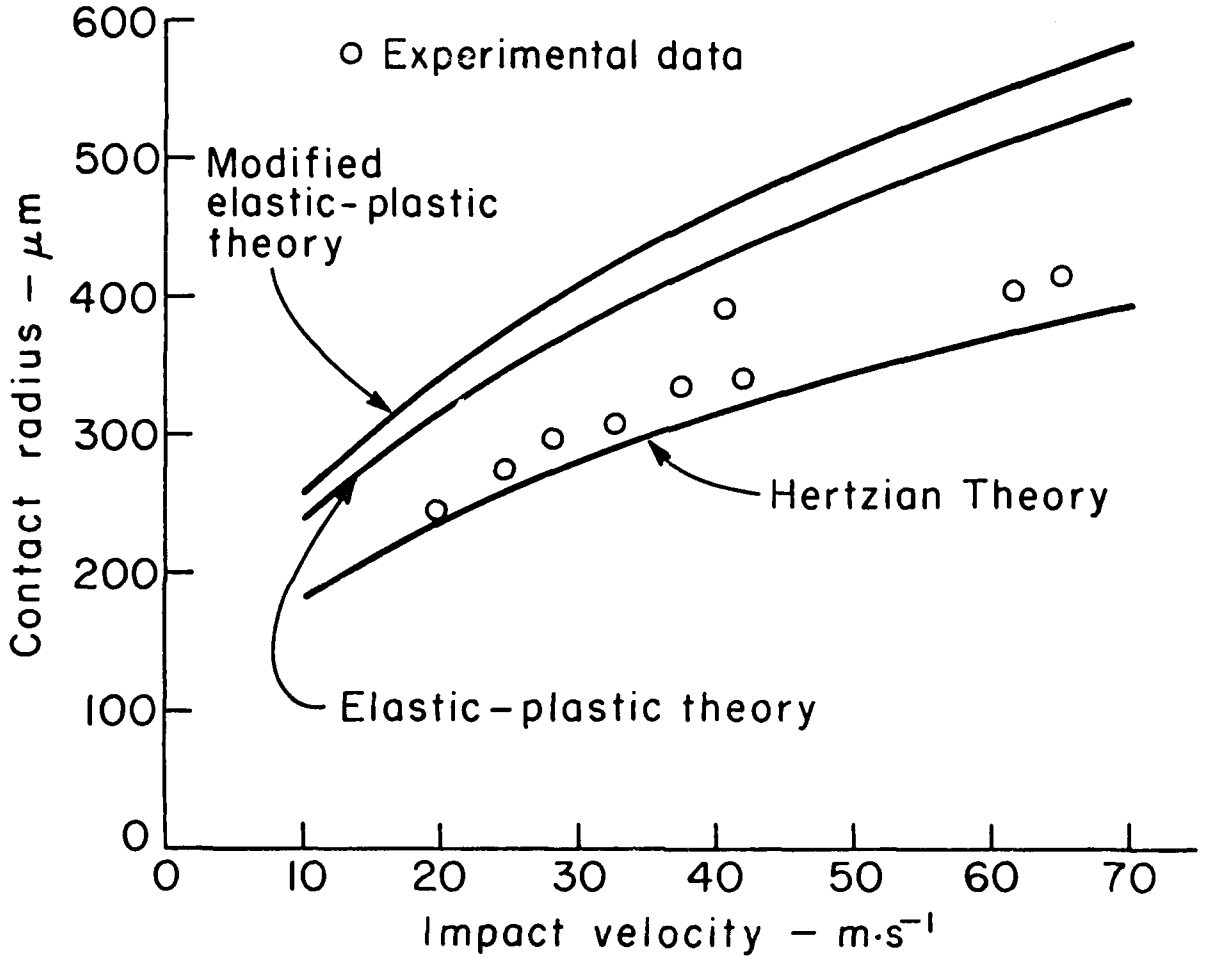

Figure 6 Contact radius vs. impact velocity (ZnS, 3 mm diameter glass spheres).

theory curve. It is interesting that this shift occurs so uniformly over the range of velocities. In this connection, it is well to remember that each impact results in a wide range of strain rates. During the early stages of the impact process the highest strain rates are encountered but these high strain rates involve a relatively small volume of material. Later in the process, the strain rates are lower and involve larger volumes of material. Apparently, the effect of averaging over these various strain rates and volumes of material is a smaller impact velocity dependence of the contact radius than might otherwise have been expected.

The impact indentation radii calculated using the elastic-plastic theory and the modified elastic-plastic theory are plotted in Figure 7 where the results are compared with the experimental data. The calculations overestimate the indentation radii mainly because the strain rate dependence of the flow stress increases the elastic response compared with that expected based on the static contact characteristics.

The predicted impact loads are plotted in Figure 8. The impact load was not measured so there are no experimental data for comparison. Therefore, comparison is made primarily with the Hertzian theory. In the elastic-plastic case, yielding occurs at the contact which decreases the average pressure in the contact compared with that expected during a completely elastic response. Yielding also increases the penetration of the sphere into the target. The net result is that the maximum impact force or load is less in the elastic-plastic case than it would be in the elastic case. The values indicated for the elastic-plastic theory seem to be too high in relation to the Hertz theory but those for the modified elastic plastic theory seem reasonable enough although we do not, as yet, have an independent means of evaluating them.

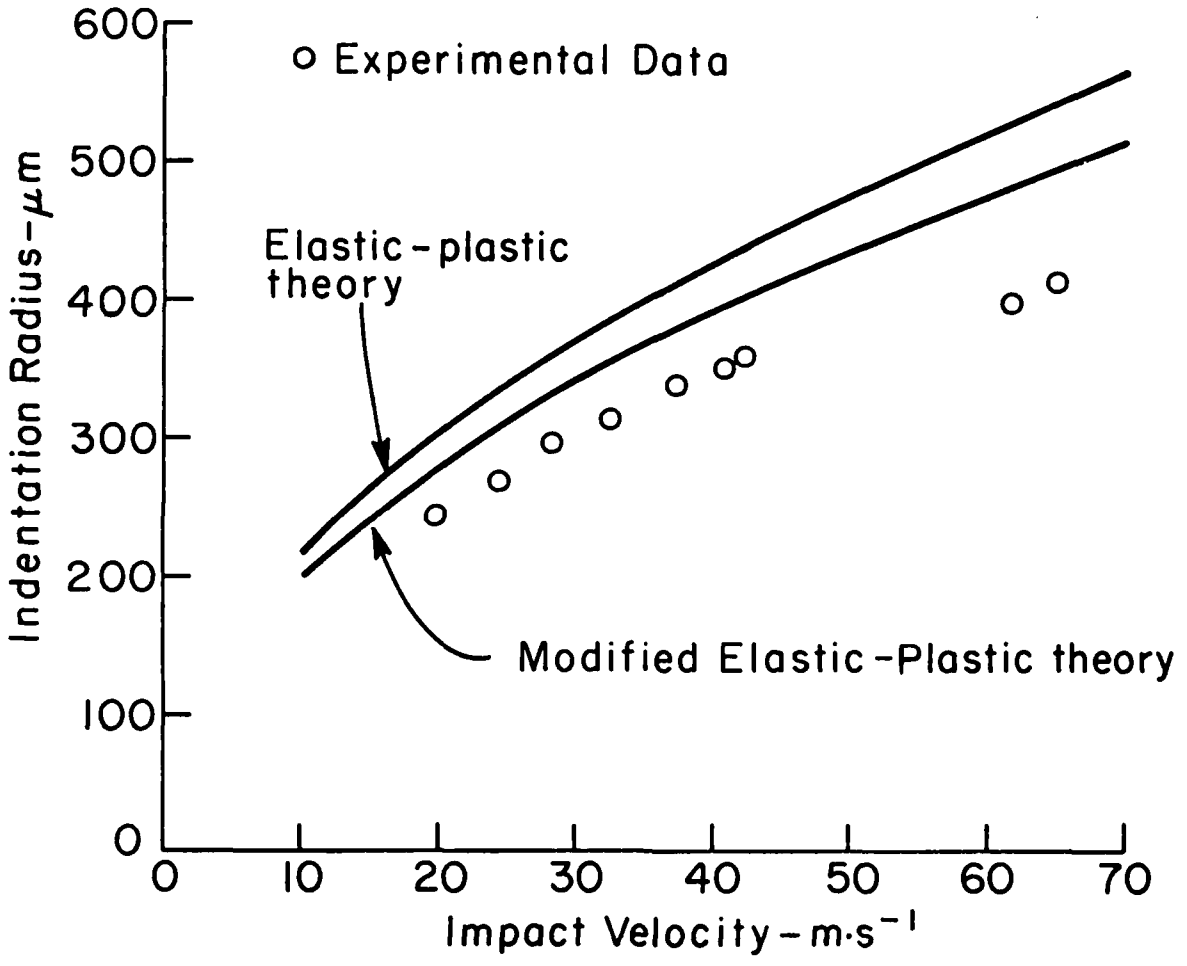

Figure 7 Comparisons of indentation radius vs. impact velocity for for elastic-plastic and modified elastic-plastic theories, and experimental data. (ZnS, 3 mm diameter glass spheres).

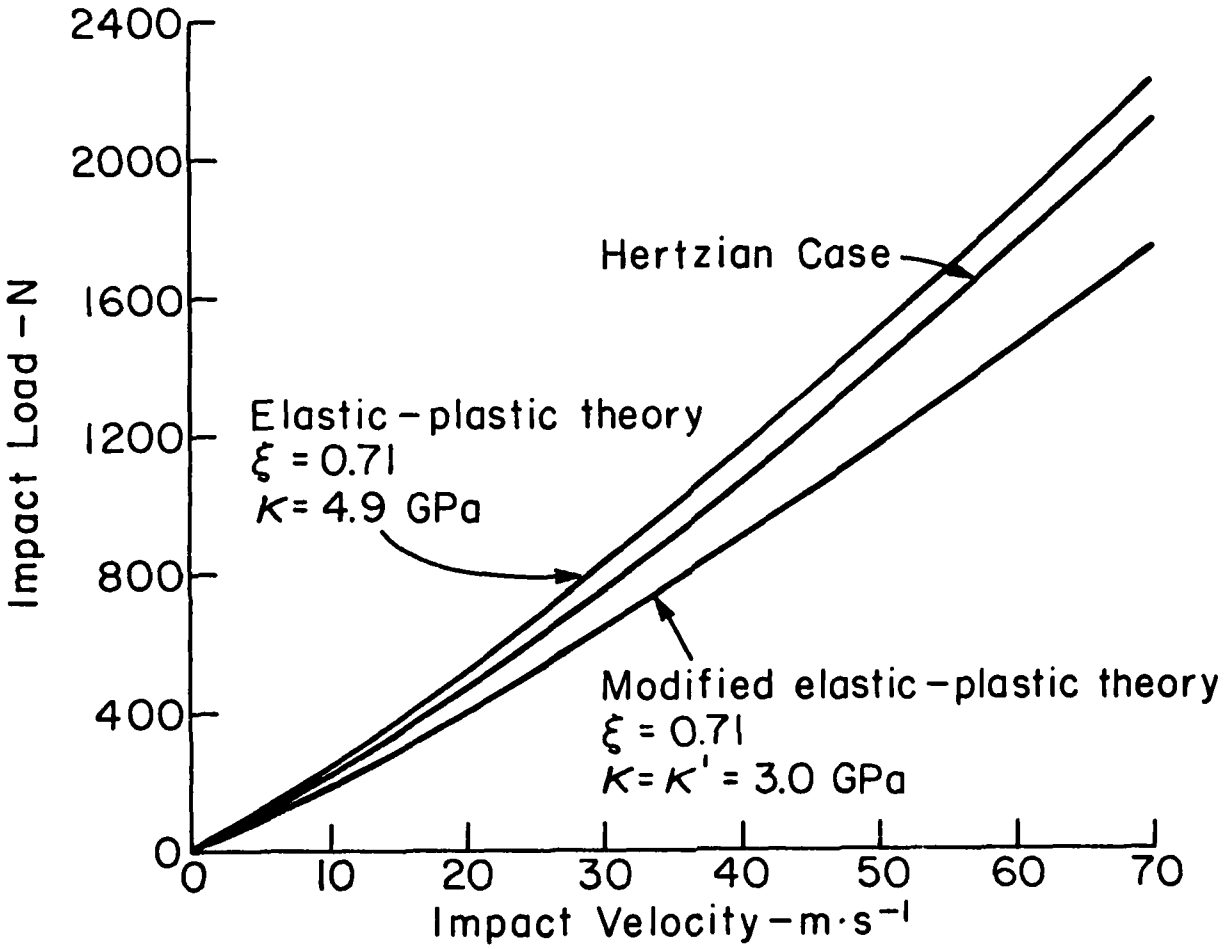

Figure 8 Comparison of the impact loads from the elastic-plastic and modified elastic-plastic theories with those calculated using the Hertzian theory. (ZnS, 3.0 mm diameter glass spheres).

One possible explanation of the high calculated values of impact load is that the theory overestimates the contact radii (Figure 6) so that the contact areas are overestimated. When these areas are multiplied by the contact pressures, the resulting load values are overestimated.

In an attempt to evaluate this effect the experimental contact radii were combined with the contact pressures to calculate the impact loads with the results shown in Figure 9. The resulting loads are about 50% as great as those represented by the theoretical curves. While this result seems reasonable there is, so far, no independent way to check this result.

For impacting spheres, the coefficient of restitution measurements provide a sensitive means to assess the energy losses that occur during the impact process. In ideal elastic impact, the sphere rebounds at the original impact velocity, the coefficient of restitution is one, and there are no energy losses. In an actual elastic impact, there are stress wave energy losses, the sphere rebounds at a velocity slightly less than the impact velocity and the coefficient of restitution is slightly less than 1, frequently in the range from 0.9 to one. In these cases, the measurement of the coefficient of restitution is a relatively sensitive means of estimating the stress wave energy. When there is an elastic-plastic response the situation becomes more complicated because both indentation energy and stress wave energy contribute to the losses and the coefficient of restitution may decline to very low values. Nevertheless, because of the sensitivity of the velocity in responding to the energy losses, coefficient of restitution measurements represent an effective means to determine how well a model corresponds to reality.

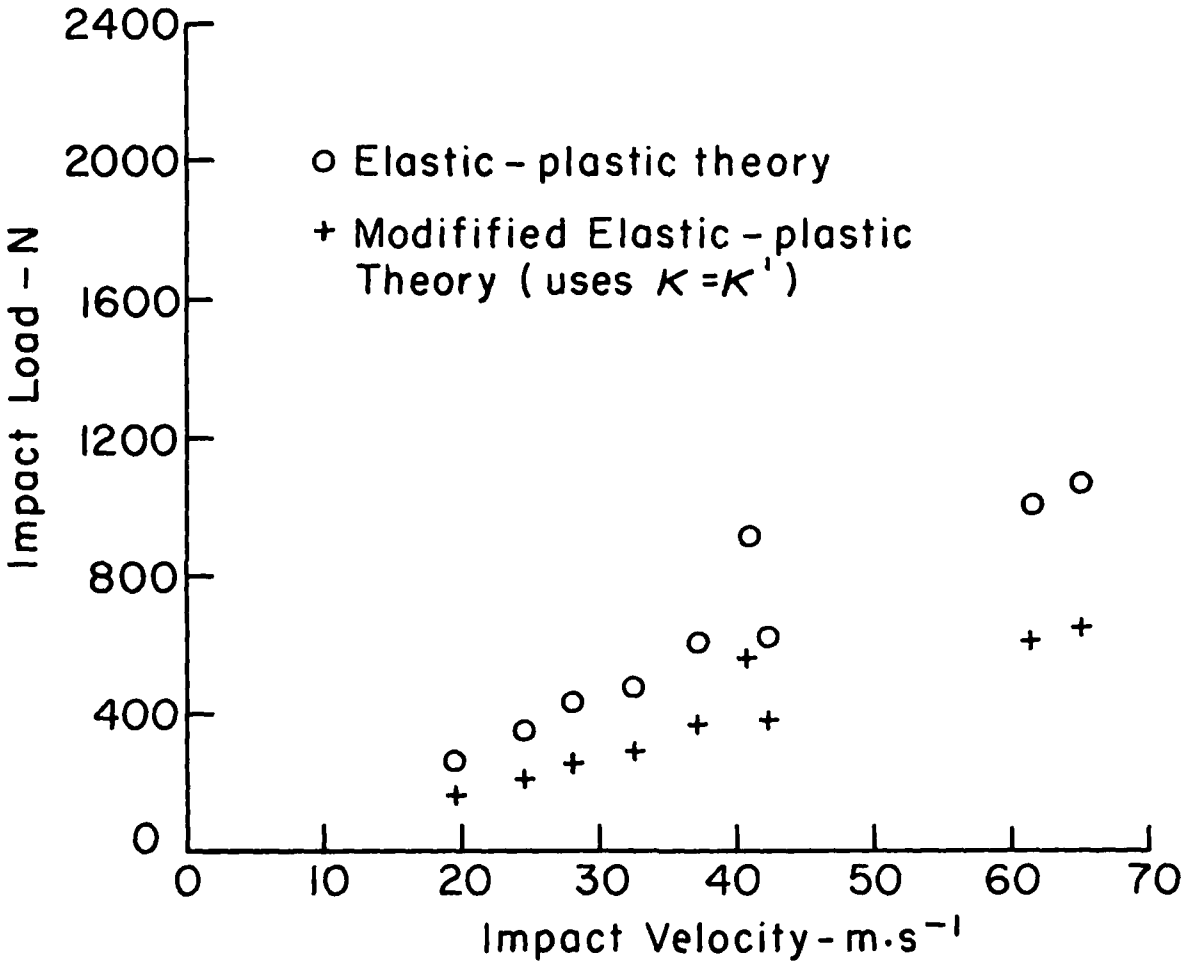

Figure 9 Impact load vs. impact velocity, using the experimental r_c values in the static relation $P = \kappa \pi r_o^{\ 2} (r_c/r_o)^{\xi+2}$ to calculate the load. (ZnS, 3 mm diameter glass spheres).

The coefficients of restitution calculated using the elastic-plastic theory and the modified theory at various velocities are plotted in Figure 10 where they are compared with the experimental data. The predicted curves greatly underestimate the measured values apparently because the strain rate dependence of the flow stress causes the material to respond much more elastically than would be predicted based on the response under static conditions.

One of the principal objectives of the present program is to predict the crack sizes and the remaining strength after impact damage. Figure 11, which is based on the relation $P/d_i \propto c^{1/2}$, was presented in a recent report[8]. The data for $c > d_c$, where d_c is the contact diameter which is used to define the boundaries of the near field, were fitted by

$$P/d_i = 2.74 \times 10^7 \, c^{1/2} + 7.87 \times 10^3 \tag{9}$$

Substituting the above equation in

$$P/d_i = \frac{1}{2} \kappa\pi r_o \left(\frac{M(\xi+4)}{2\kappa\pi r_o^3}\right)^{\frac{(\xi+2)(\xi'+1)}{(\xi+4)(\xi'+2)}} \left(\frac{2(\xi+2)(\xi'+1)}{(\xi+4)(\xi'+2)}\right) V_o \tag{10}$$

yields an equation that can be used to predict radial crack length. The results of these theoretical calculations are compared with the experimental data in Figure 12. Although the modified theory yields an improvement in the fit to the experimental data, it is clear that the theory still does

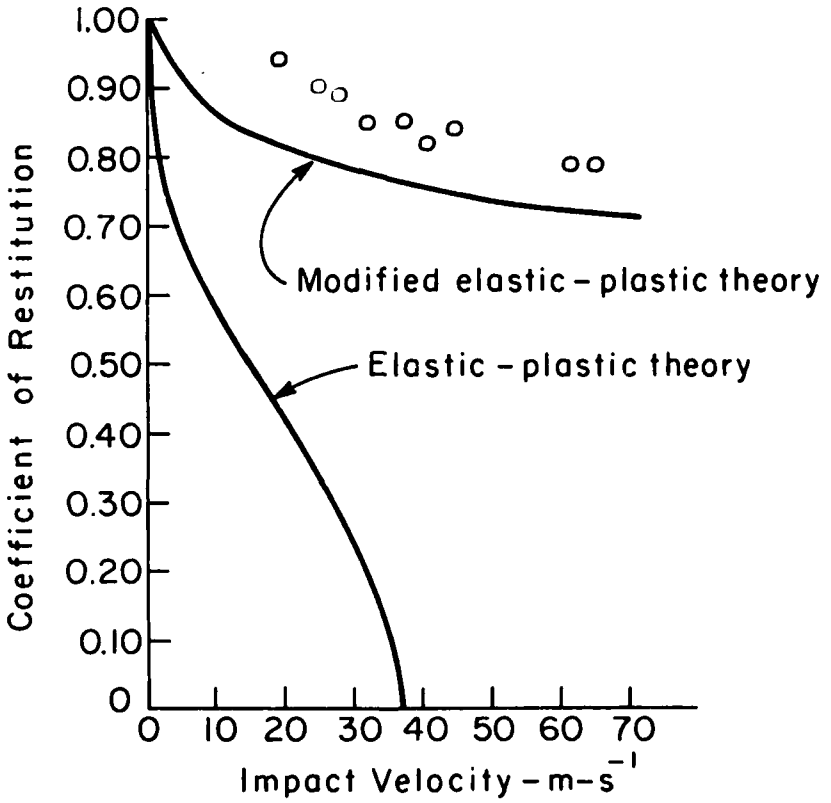

Figure 10 The coefficient of restitution v.s. the impact velocity. (CdS impacted by 3 mm diameter glass spheres).

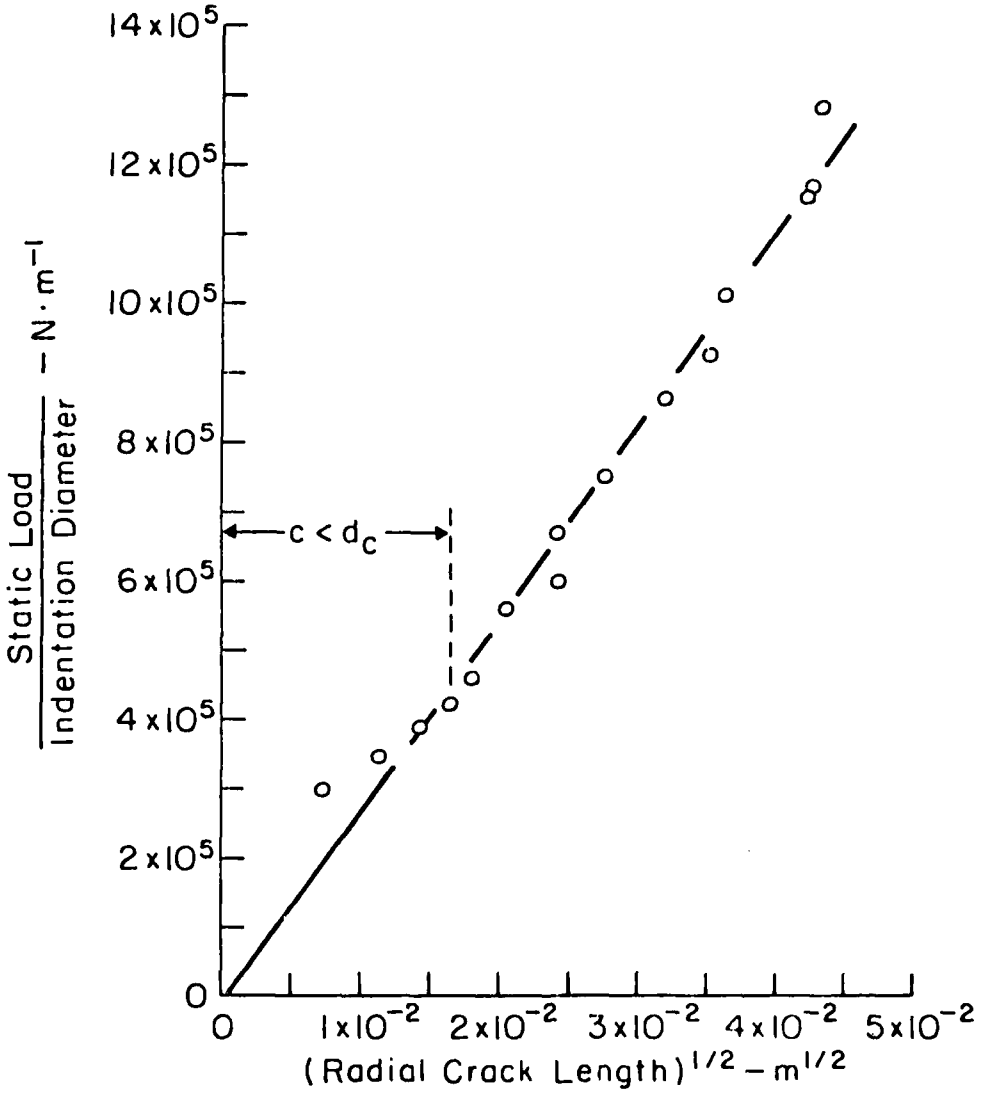

Figure 11 Static load divided by the indentation diameter vs. radial crack length measured from the edge of the indentation and raised to the 1/2 power (ZnS, 3 mm diameter glass spheres).

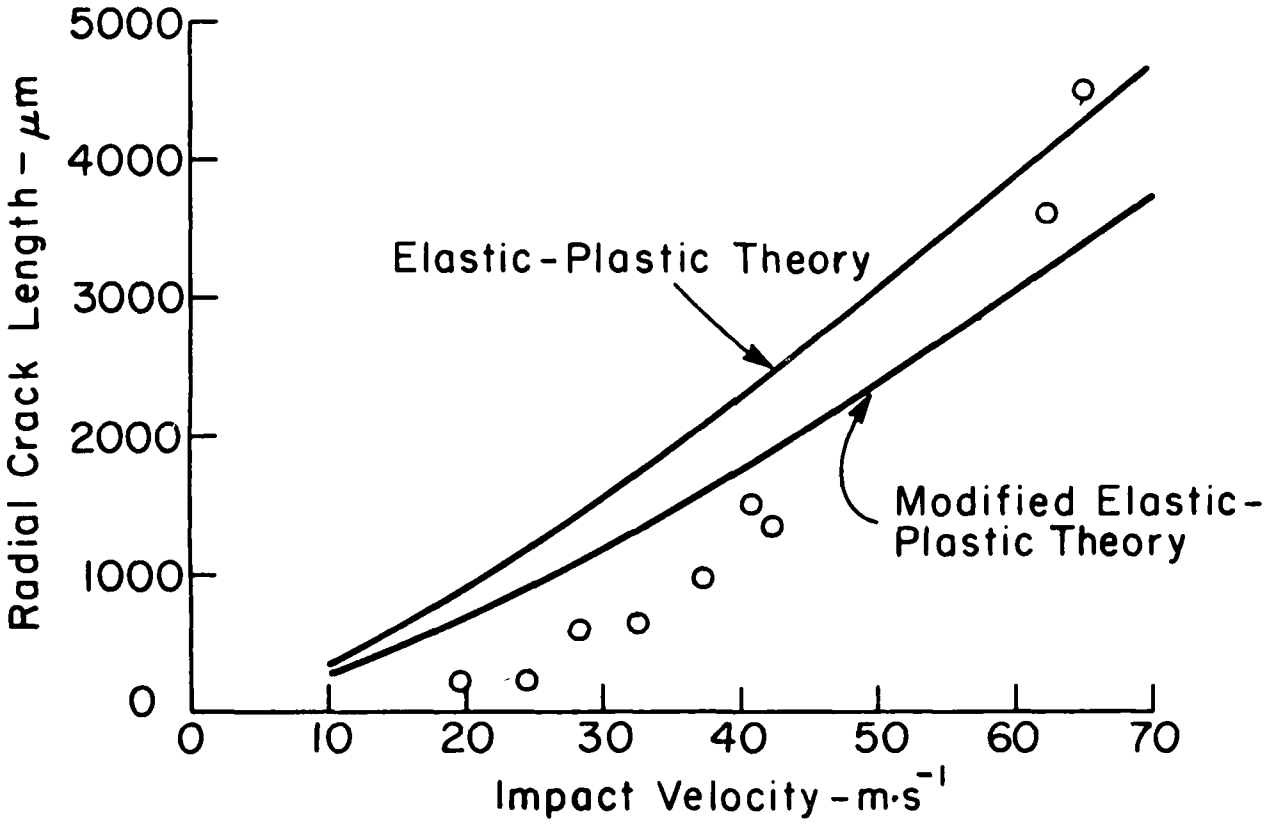

Figure 12. Radial crack length vs. impact velocity for the elastic-plastic theory and the modified elastic-plastic theory of Hertzian fracture (9) and (10). (ZnS; 3.0 mm diameter glass spheres).

not account for the strong variation in maximum radial crack length with impact velocity represented by these data.

Tungsten Carbide Spheres on TT-ZrO_2

Impacts of tungsten carbide spheres on TT-ZrO_2 yield an elastic-plastic response despite the fact that zirconia is much harder than zinc sulfide. The log contact pressure vs log normalized contact radius curves for the three grades of TT-ZrO_2 show leveling off of the contact pressure at normalized contact radius values above 0.21. This behavior was not observed in the other materials. Also, it was not observed in the indentation radius measurements on TT-ZrO_2. The mechanism responsible for the behavior is not understood. The possibility that it might occur as a result of plastic deformation of the sphere was considered. The spheres were examined by optical microscopy and no evidence of plastic deformation was observed. However, it is quite possible that small plastic deformations could have gone undetected. Another possibility is that it might be caused by a phase transformation, perhaps monoclinic to tetragonal under the very high pressure conditions existing under the contact. With regard to both of these mechanisms, it is not clear why the leveling off is observed only in the contact pressure and not in the indentation pressure.

The contact characteristics measured for the three grades of TT-ZrO_2 can be compared (Table IV). Although there seem to be systematic variations, in view of the uncertainties in the results, these variations may not be significant. The indentation radii observed at various static loads on as-fired and peak-aged TT-ZrO_2 are compared in Figure 13. Little difference was observed in the results for the two materials. Therefore, the aging

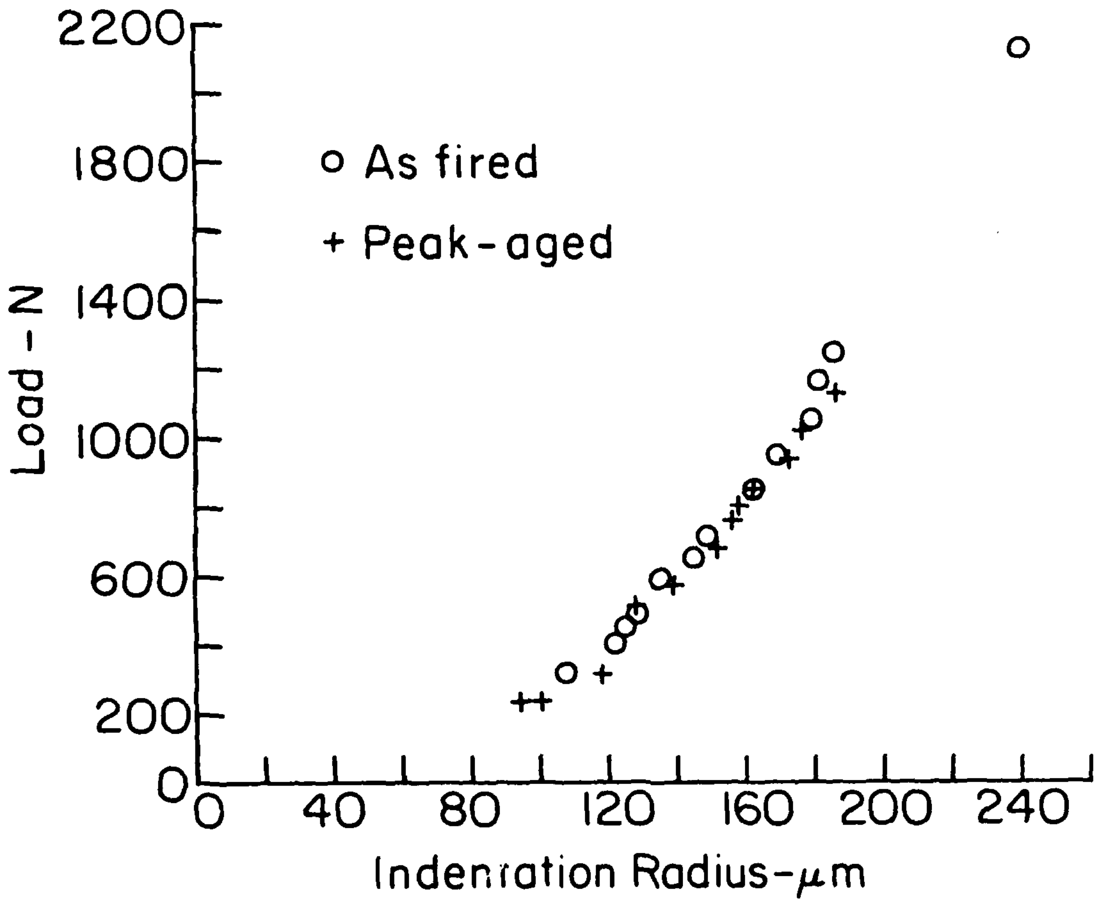

Figure 1[illegible]. Load vs. indentation radius for as-fired and peak-aged TT-Zr[illegible].
([illegible] mm diameter WC sphere).

treatment does not seem to have an appreciable effect on the plastic flow properties of TT-ZrO_2.

The contact radius vs impact velocity predictions are plotted in Figures 14-16 where they are compared with experimental data. Because the measured contact radii increase with the thickness of the soot layer but the theory is based on the actual contact with the specimen surface, it seems reasonable to give added weight to the lower contact radius values in interpreting these results. Using this approach, the original and modified elastic-plastic theories overestimate the contact radii. Again, it seems likely that the contact radii are smaller than expected because the strain rate dependence of the flow stress causes the TT-ZrO_2 to respond more elastically than expected based on the contact parameters determined during static loading. It is also possible that the data are slightly underestimated as a result of the elastic contraction of the load is removed. The Hertzian theory underestimates the contact radii in each case as expected.

The indentation radius vs impact velocity predictions are plotted in Figures 17-19 where they are compared with experimental data. In each case, the predictions overestimate the indentation radii. Again, it seems likely that the variation in flow stress with strain rate is causing the material to respond more elastically than it does during static indentation.

The predicted impact load values are plotted versus impact velocity in Figures 20-22. The loads, calculated using the elastic-plastic and the modified elastic-plastic theories, are higher than the Hertzian theory values reflecting the fact that the contact radii are overestimated as

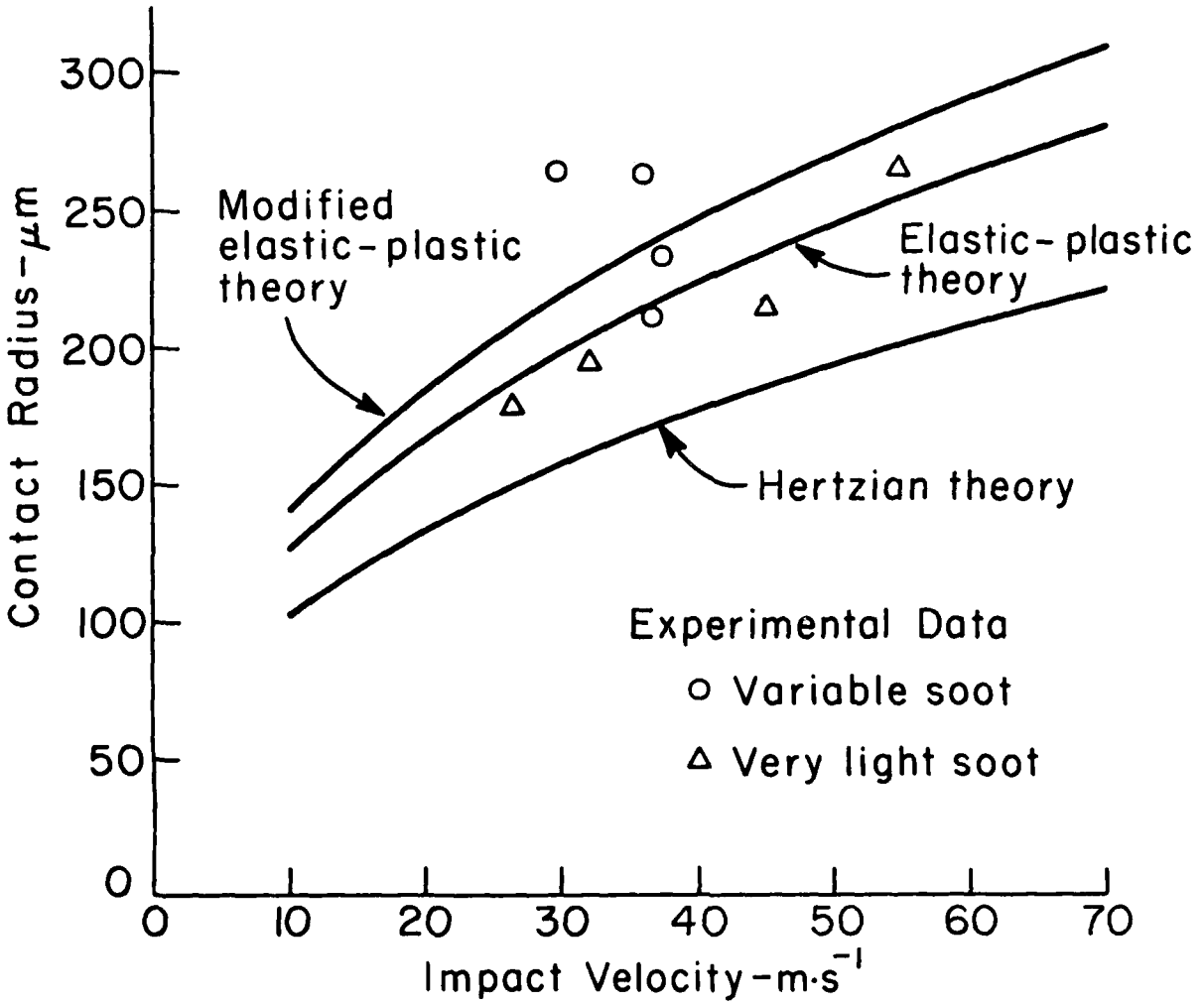

Figure 14. Contact radius vs. impact velocity (air fin I Y_2O_3, 1.59 mm diameter tungsten carbide sphere).

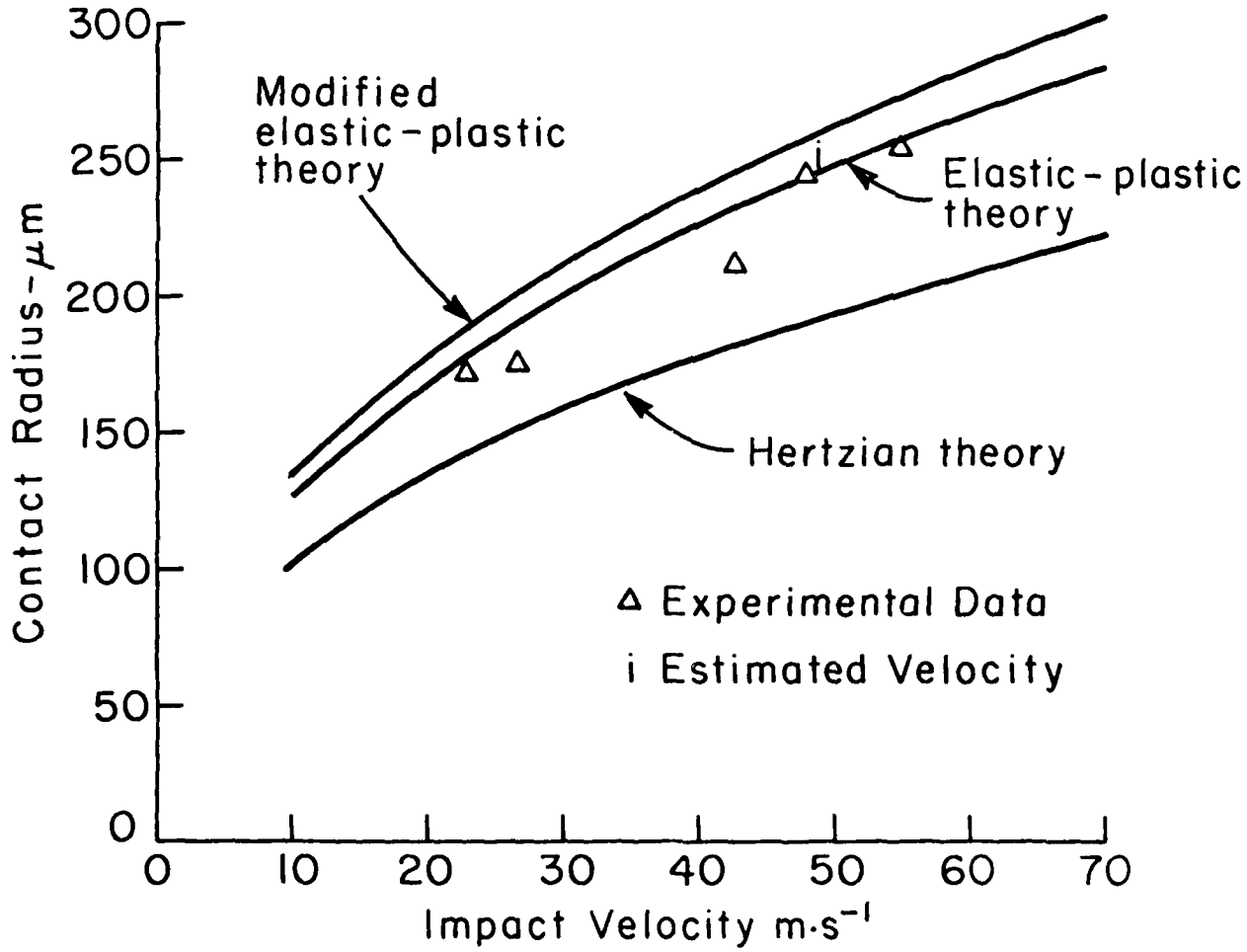

Figure 15. Contact radius vs. impact velocity (upper-ascent 9%-Co , 1.59 mm diameter tungsten carbide spheres).

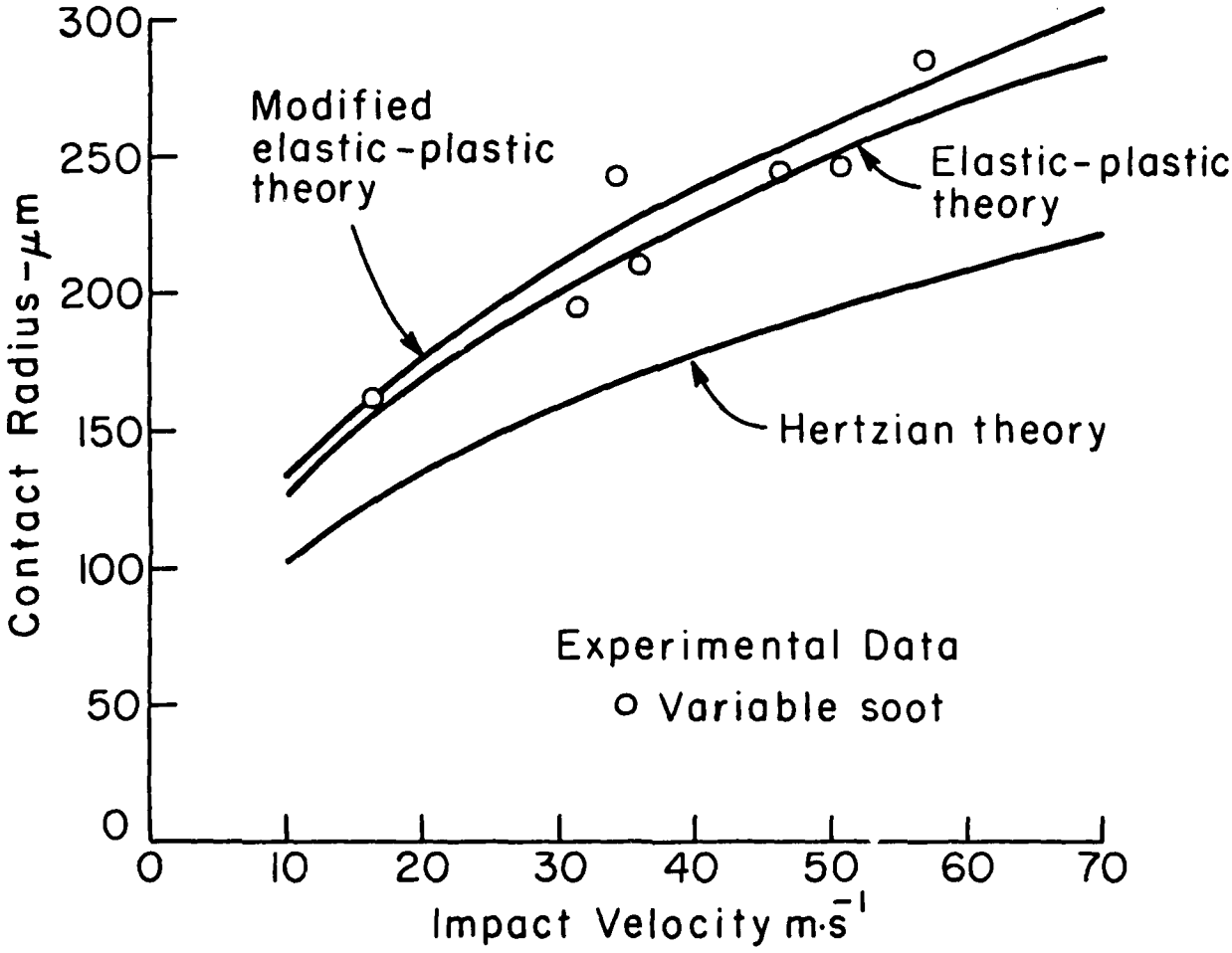

Figure 16 Contact radius vs. impact velocity (peak-aged TT ZrO_2, 1.59 mm diameter tungsten carbide spheres).

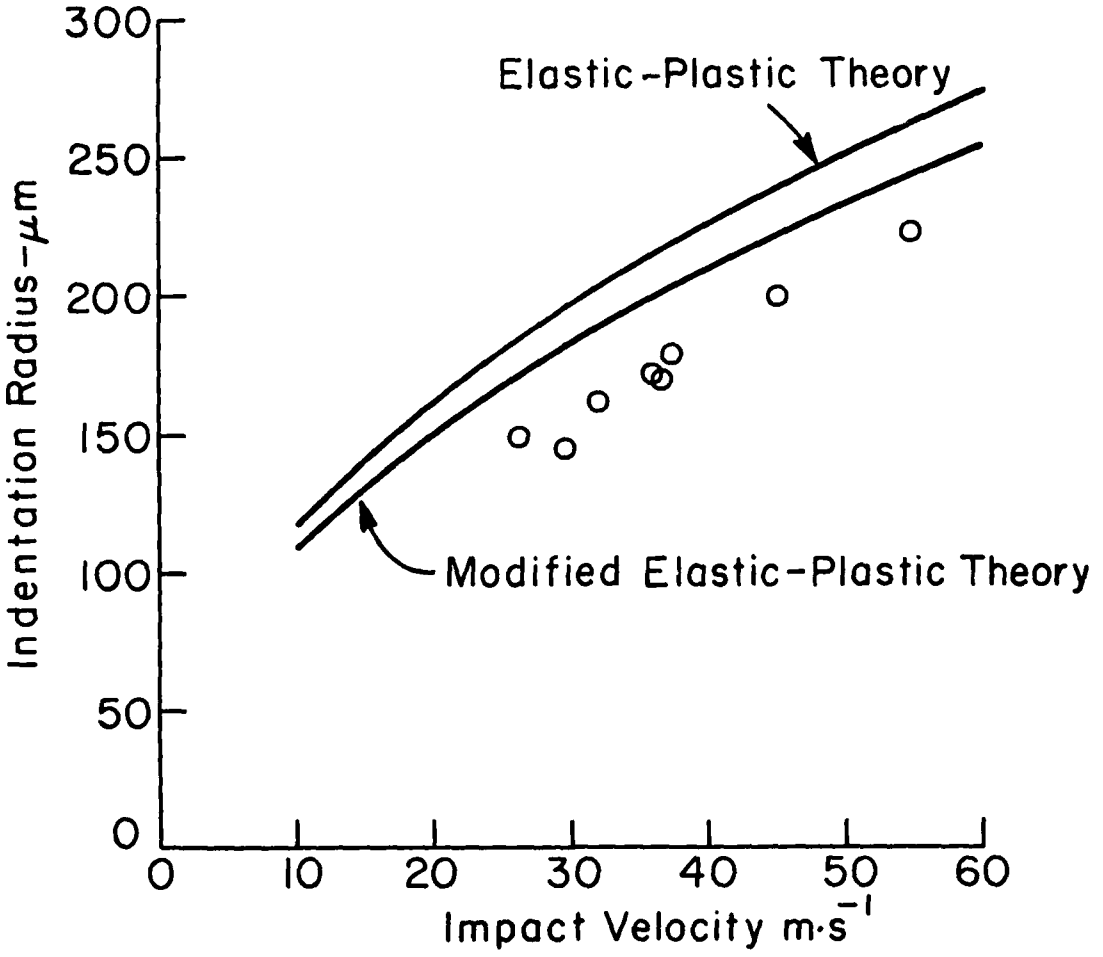

Figure 17 Comparison of indentation radius vs. impact velocity for the elastic-plastic and modified elastic-plastic theories and experimental data (as-fired TT-ZrO_2; 1.59 mm diameter tungsten carbide spheres).

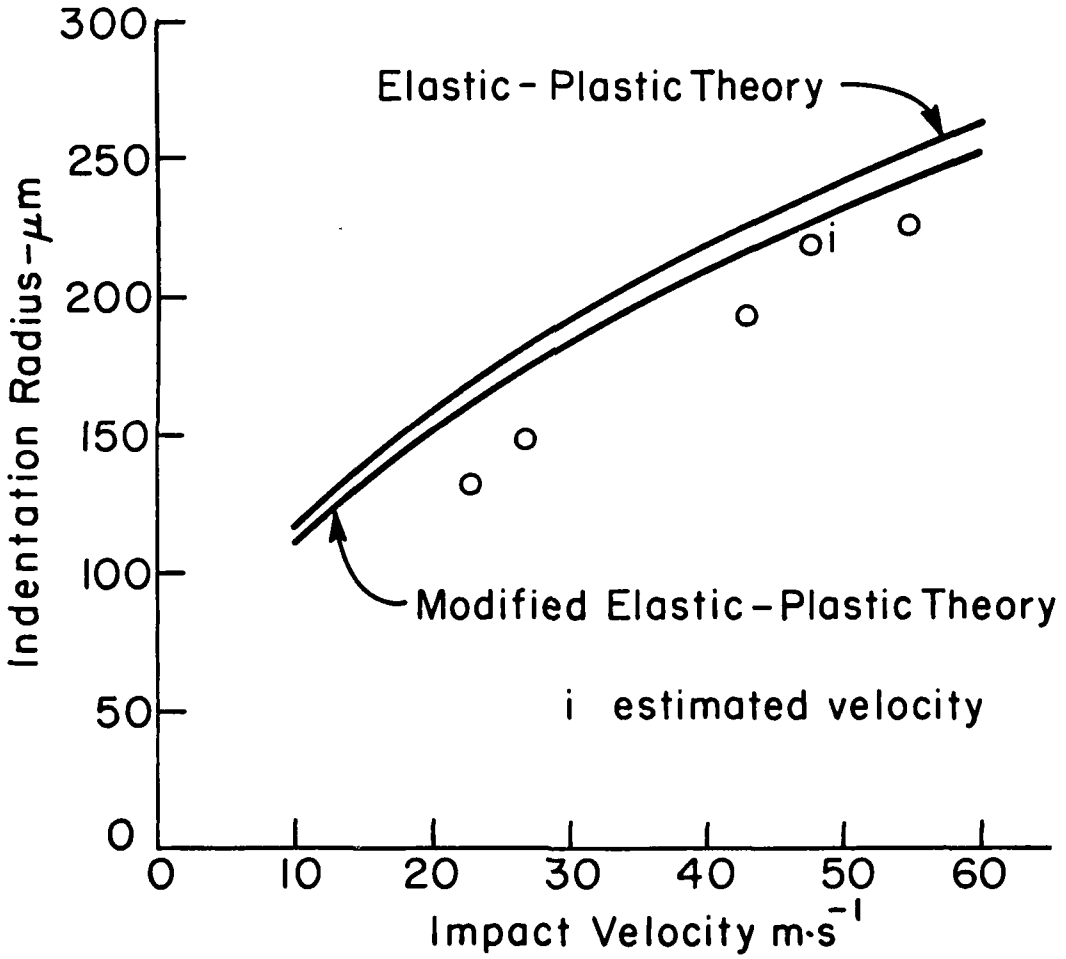

Figure 18 Comparison of indentation radius vs. impact velocity for the elastic-plastic and modified elastic-plastic theories and experimental data (under-aged TT-ZrO_2; 1.59 mm diameter tungsten carbide spheres).

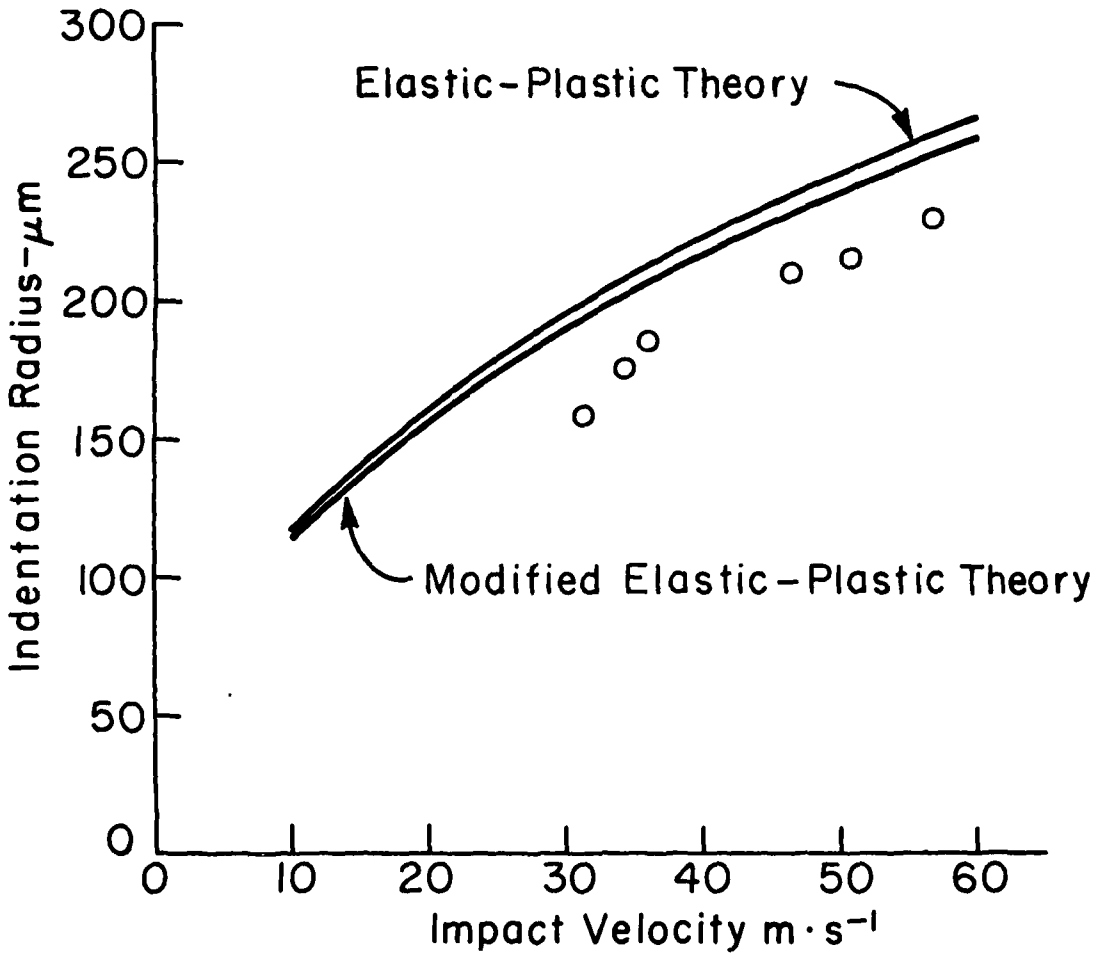

Figure 19 Indentation radius vs. impact velocity for the two elastic-plastic theories (original and modified) with experimental data (peak-aged TT-ZrO_2; 1.59 mm diameter tungsten carbide spheres).

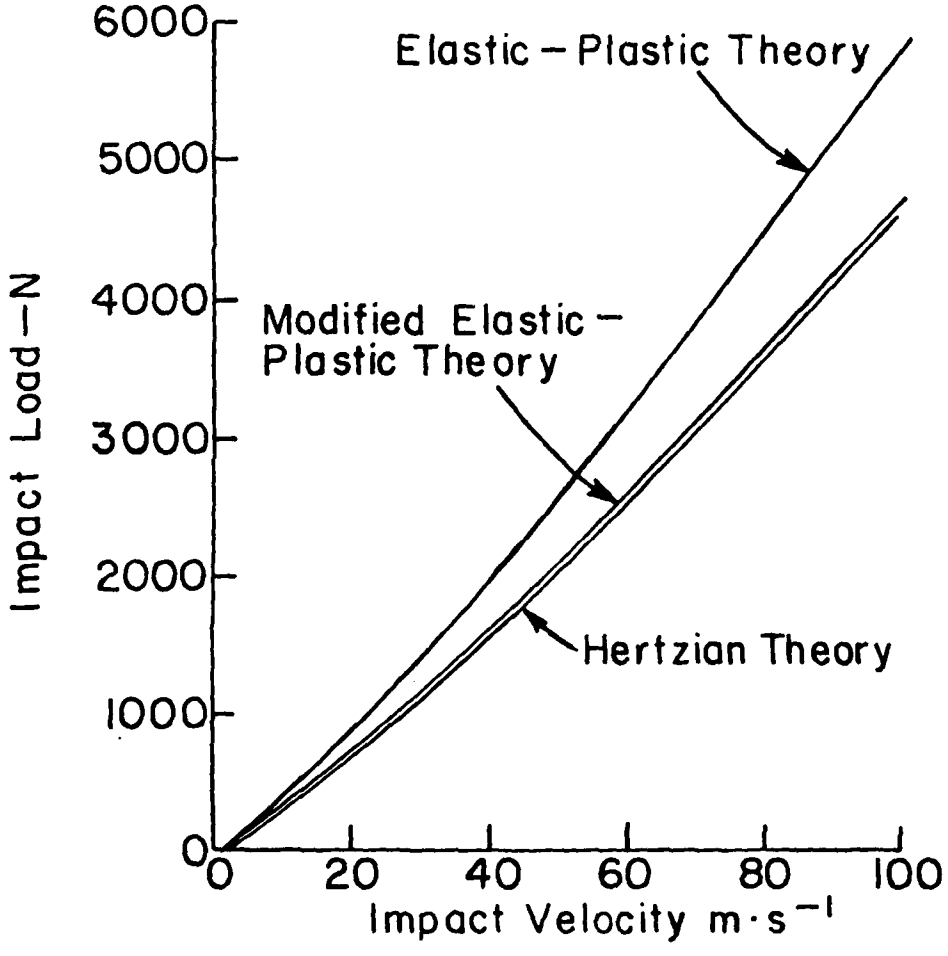

Figure 30 Impact load vs. impact velocity for three theories (as-fired TT-ZrO_2, 1.59 mm diameter tungsten carbide spheres).

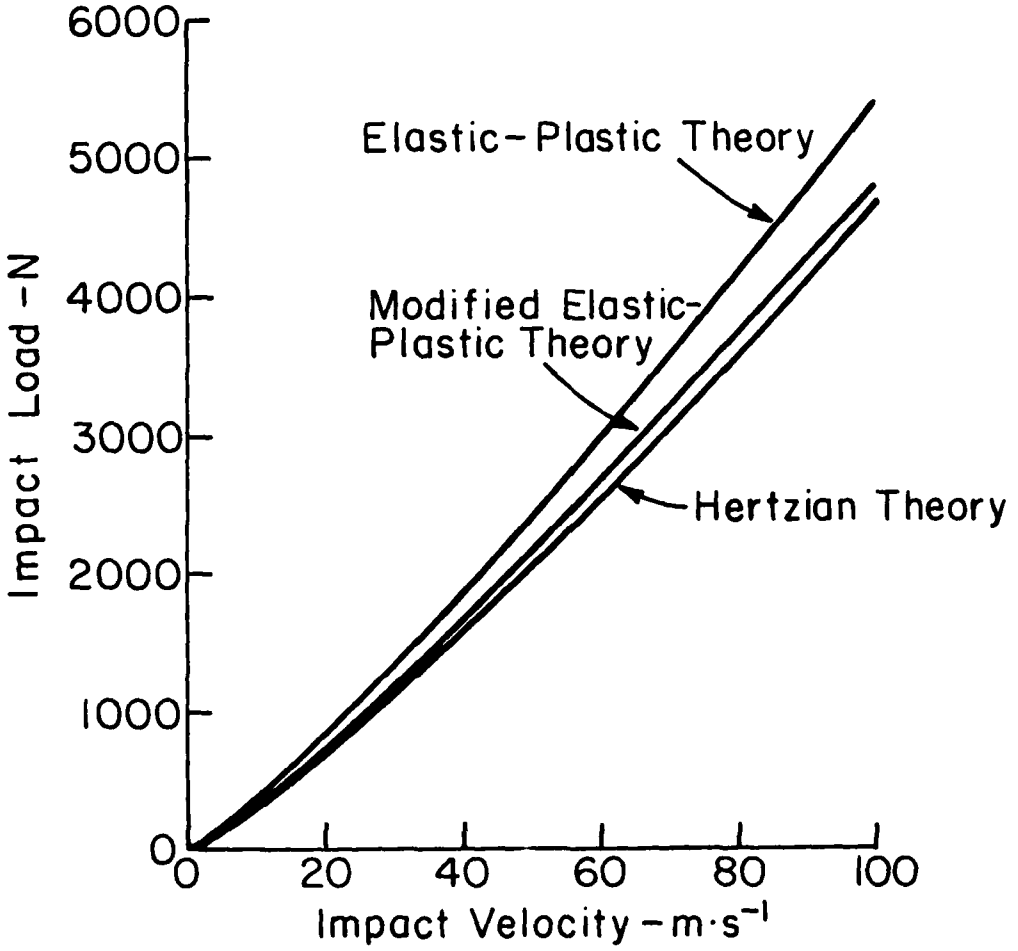

Figure 1. Impact load vs. impact velocity for three theories (nylon-coated steel, 1.59 mm diameter tungsten carbide spheres).

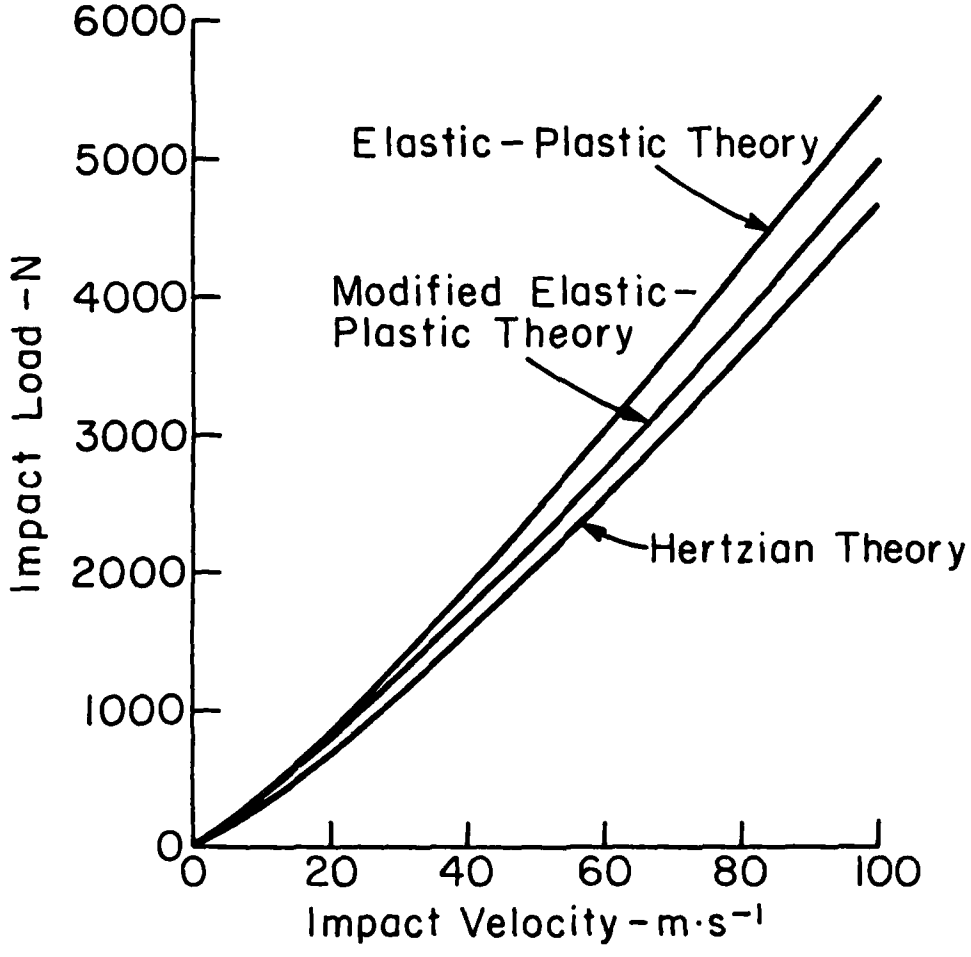

Figure 9. Impact load vs. impact velocity for three theories (peak-aged TT-ZrO_2, 1.59 mm diameter tungsten carbide spheres).

shown in Figures 14-16 so that when the contact pressures are summed over the contact area, the loads are overestimated. As in the case of ZnS, one way to obtain more realistic estimates is to use the experimental (impact) contact radii together with the experimental contact characteristics κ and ξ to estimate the load. However, unlike the case of ZnS, when this was done the loads calculated using the elastic-plastic theory did not show the expected reduction.

As mentioned previously, the coefficient of restitution responds very sensitively to the variations in the energy absorption mechanisms. In Figures 23-25, predicted values of coefficient of restitution at various impact velocities are compared with experimental data. Again, the modified theory yields the best results mainly because in this case the κ/κ' ratio is one whereas in the original theory $\kappa/\kappa' > 1$ and the results are very sensitive to this value.

The radial crack lengths were measured in the surfaces of the statically loaded TT-ZrO_2 specimens, from the edge of the indentation to the tip of the longest crack. The results are plotted as suggested by $P/d_i \propto c^{1/2}$ in Figures 26 and 27. The data for the as fired TT-ZrO_2, plotted in Figure 26, show a linear variation and the data points for $c > d_i$ fit the line

$$P/d_i = 7.93 \times 10^5 + 1.43\, c^{1/2} \qquad (11)$$

with a coefficient of determination of 0.995. The data points for $c < d_i$ were not used for the computation because near the contacts the crack lengths are considered to be transitional and may vary because of other characteristics of the contacts.

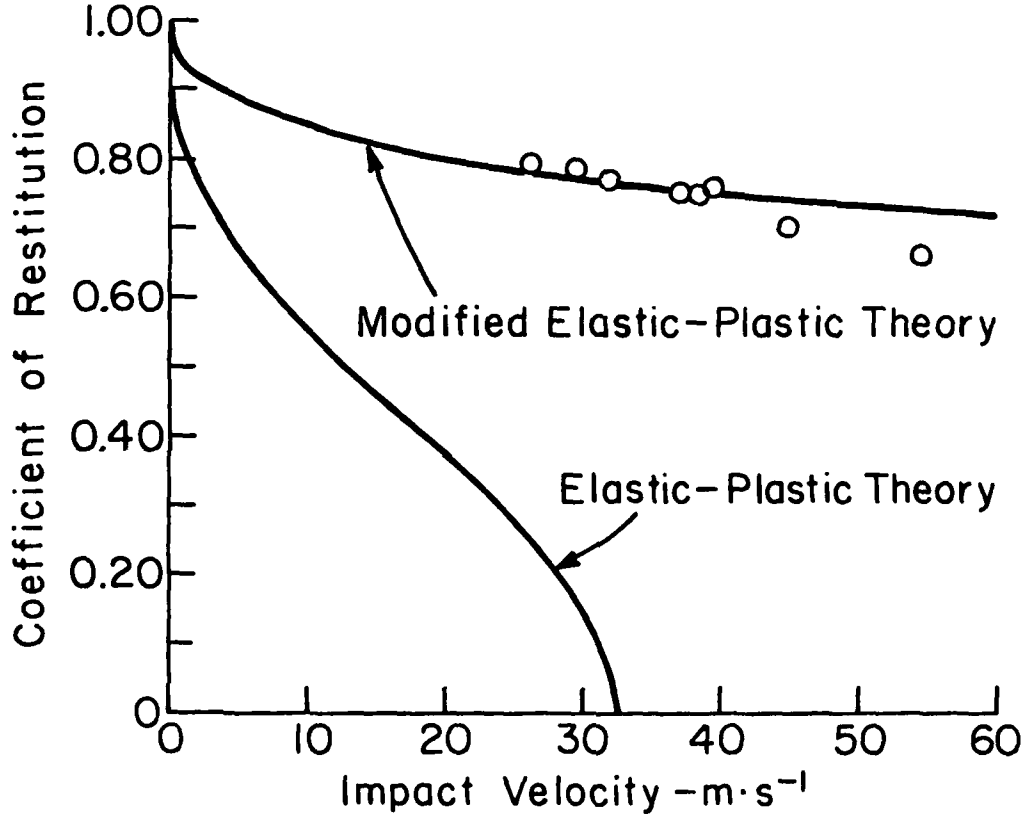

Figure 4. Comparison of two theoretical coefficient of restitution vs. impact velocity curves with experimental data (as-fired TT-2r6), 1.59 mm diameter tungsten carbide spheres).

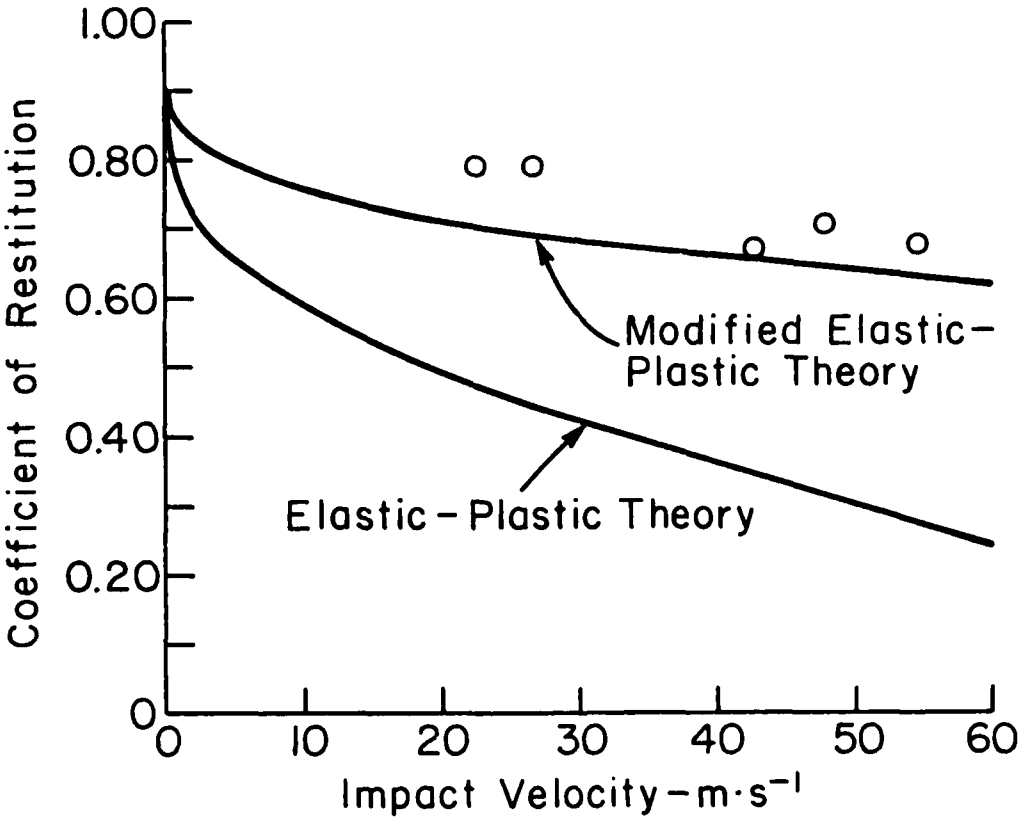

Figure 24. Comparisons of two theoretical coefficient of restitution vs. impact velocity curves with experimental data (under-sized WC-Co, 1.59 mm diameter tungsten carbide spheres).

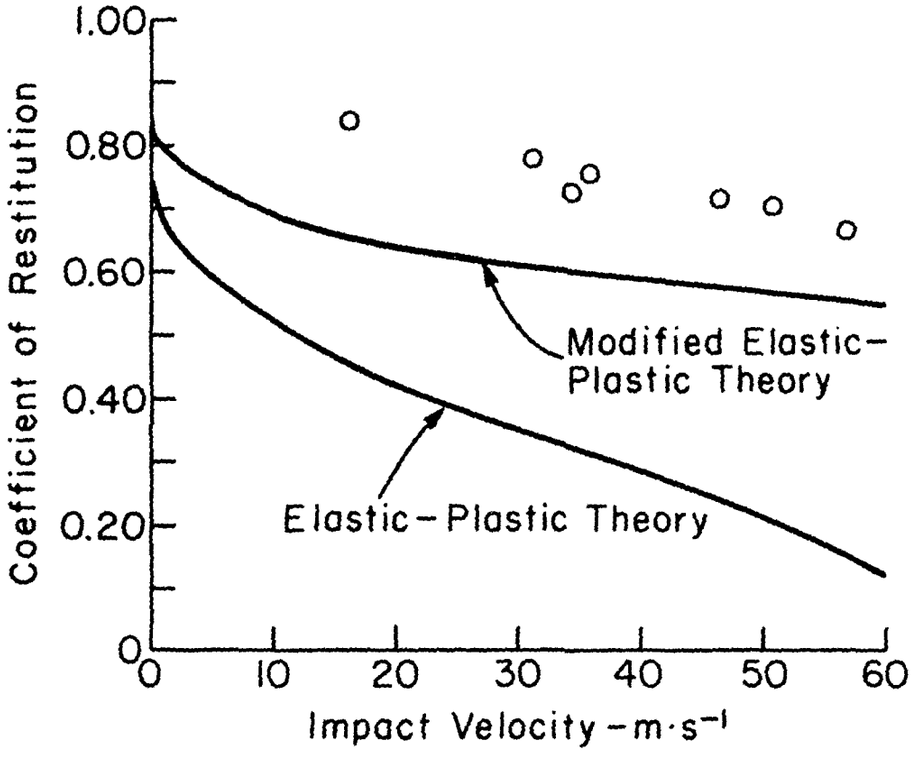

Figure 7. Comparison of two theoretical coefficient of restitution vs. impact velocity curves with experimental data (aluminum alloy 1.59 mm diameter tungsten carbide sphere).

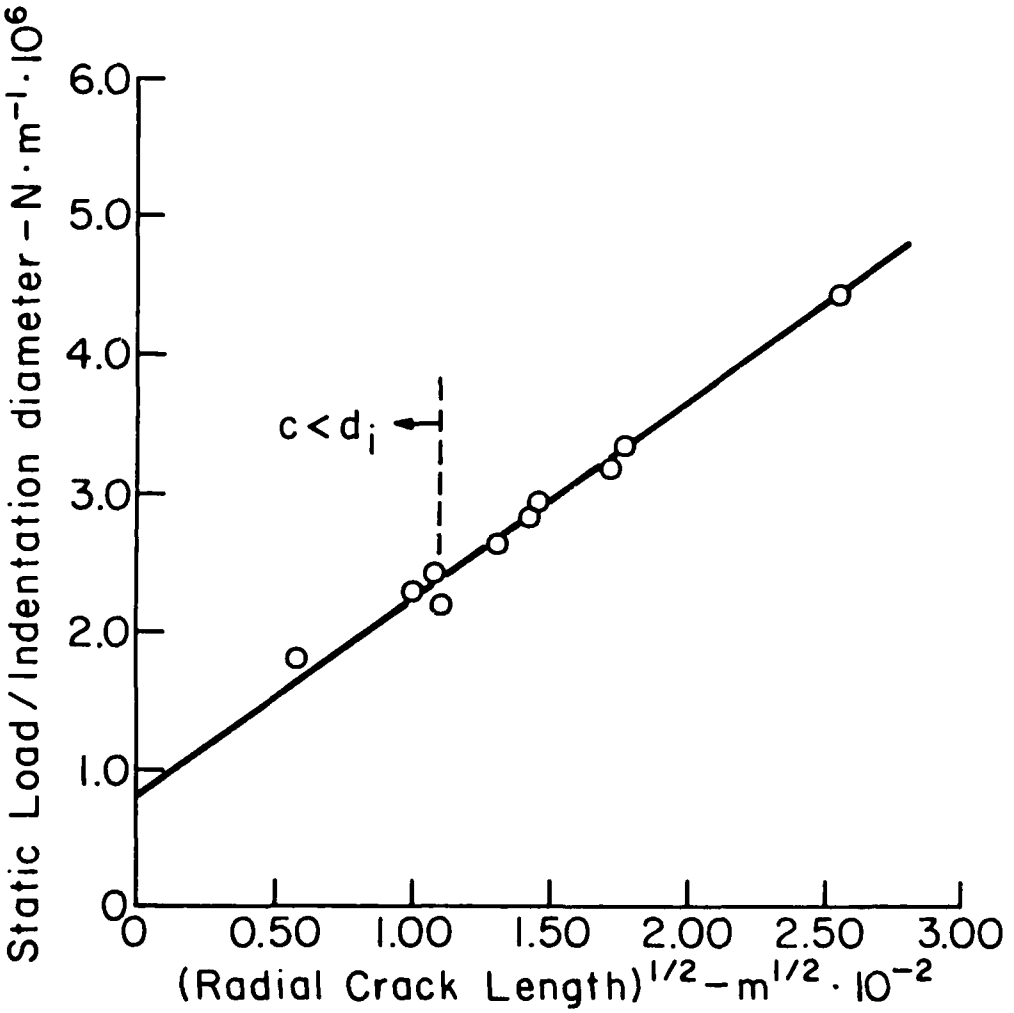
Static Load / Indentation diameter – N · m⁻¹ · 10⁶
6.0
5.0
4.0
3.0
2.0
1.0
0
c < d_i
0
0.50
1.00
1.50
2.00
2.50
3.00
(Radial Crack Length)^1/2 – m^1/2 · 10⁻²

The line does not extrapolate through the origin but instead intercepts the vertical axis at an appreciable load. In this respect the as-fired TT-ZrO_2 is somewhat different from the ZnS. This difference has not yet been explained.

The data for the as-fired, under-aged and peak-aged specimens are compared in Figure 27. Although the data are somewhat sparse and scattered, the results fail to show the expected decrease in crack length with increasing K_{Ic} that occurs as a result of aging. The K_{Ic} values ranging from 4.5 to 6.5 $MPam^{1/2}$ were expected to yield a two to one variation in crack lengths.

The failure to benefit from increased K_{Ic} with aging in TT-ZrO_2 was reported previously[10]. In that case it was found that the number of radial cracks decreased with increasing aging. New data supporting this observation are presented in Figure 28. It is well known that the stress intensity factor at a group of radiating cracks decreases with increasing number of cracks (decreasing spacing). Therefore, it is reasonable to expect that the increased number of cracks in the materials with lower K_{Ic} might serve to limit the crack propagation compared with that otherwise expected, yielding results like those shown in Figure 27.

Another possible explanation is that residual stresses increase radial crack propagation and that the residual stresses increase with increased aging, thus offsetting the effect of the increased K_{Ic}. This argument is contradicted by the fact that there is no appreciable variation in plastic flow properties with aging (Figure 13).

Using the statically determined crack length relation (Equation 11) together with equation (10), the theoretical crack length vs impact velocity

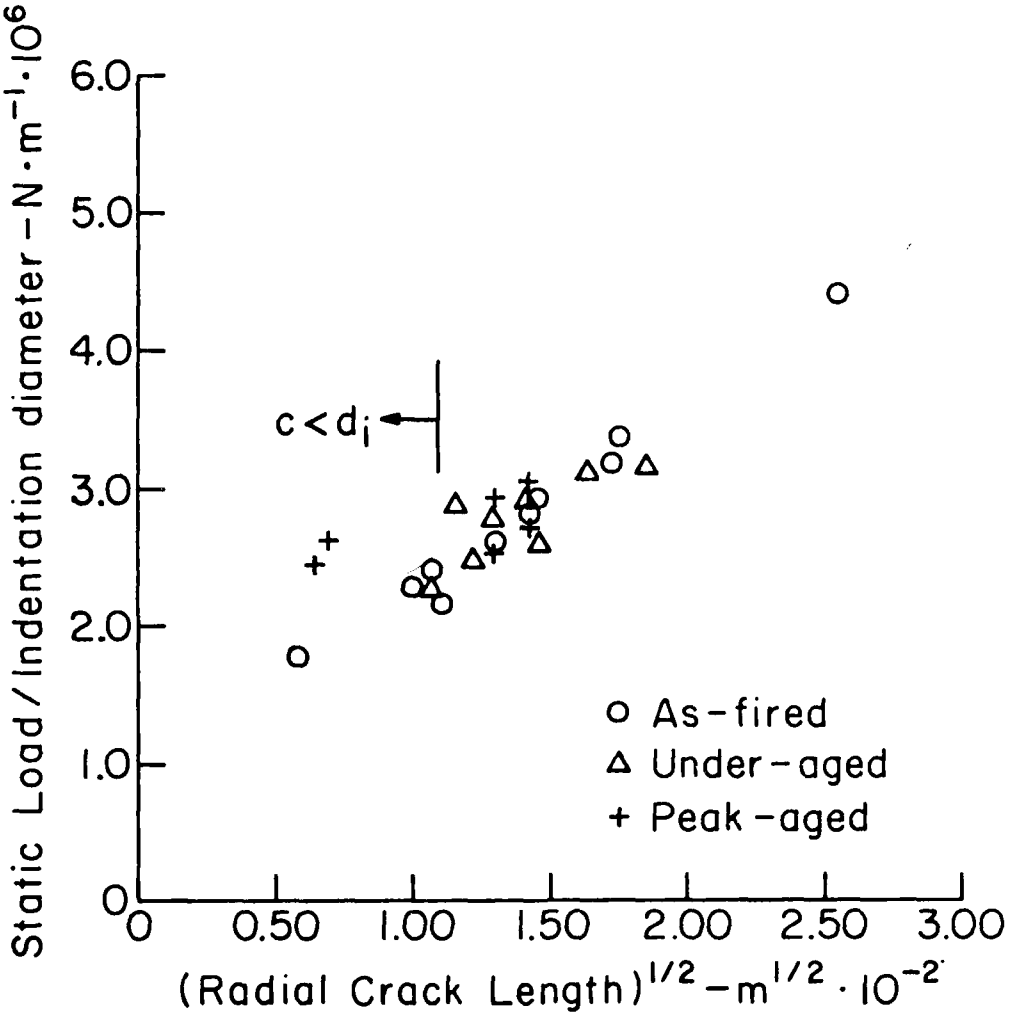

Figure 7. Static load divided by the indentation diameter vs. radial crack length to the 1/2 power for as-fired, under-aged (7 hr), (1/2 mm diameter indenter, variable cycles).

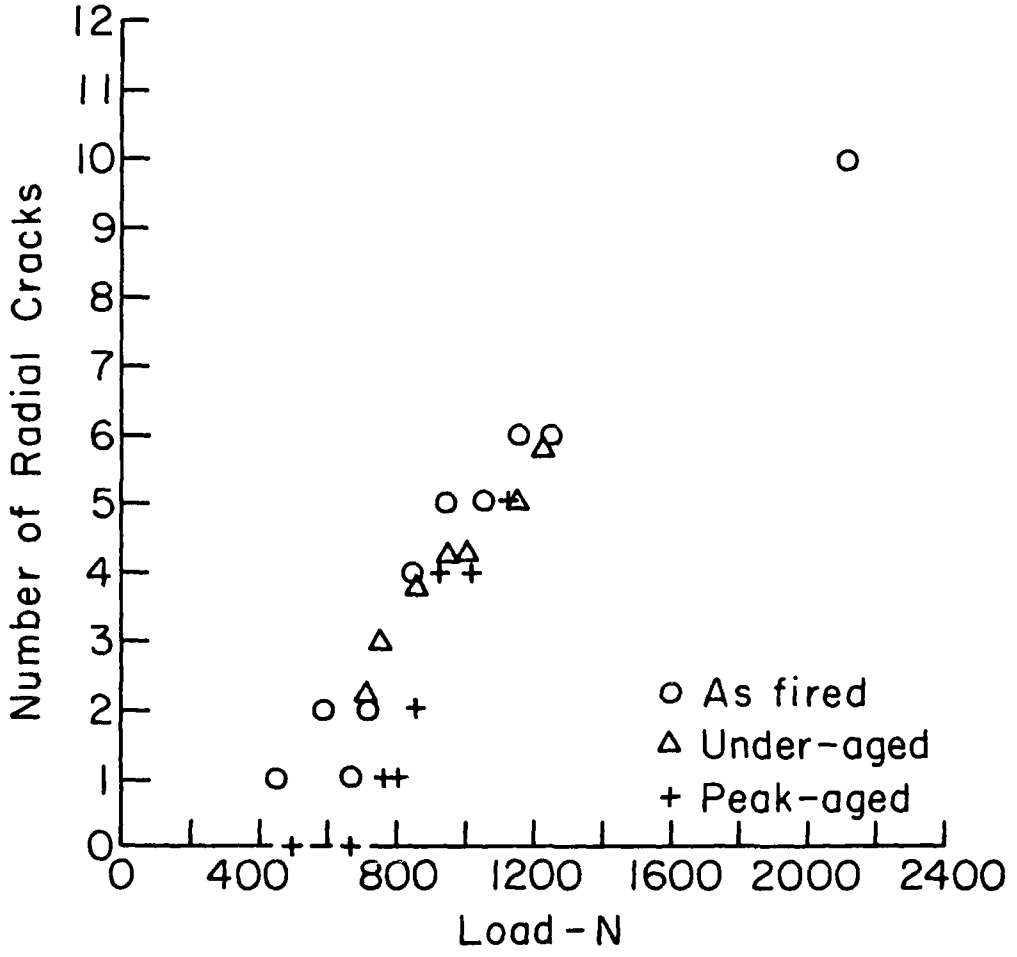

Figure 24. Number of radial cracks vs. load for three aging treatments of PY-ZrO$_2$ yielding different K_{Ic} values (1.59 mm diameter tungsten carbide spheres).

curves were plotted and compared with the experimental data in Figure 29. The original elastic-plastic theory drastically overestimates the crack lengths. However, the modified theory yields much more reasonable results, slightly overestimating the crack lengths at low velocities and underestimating the crack length at the highest velocity.

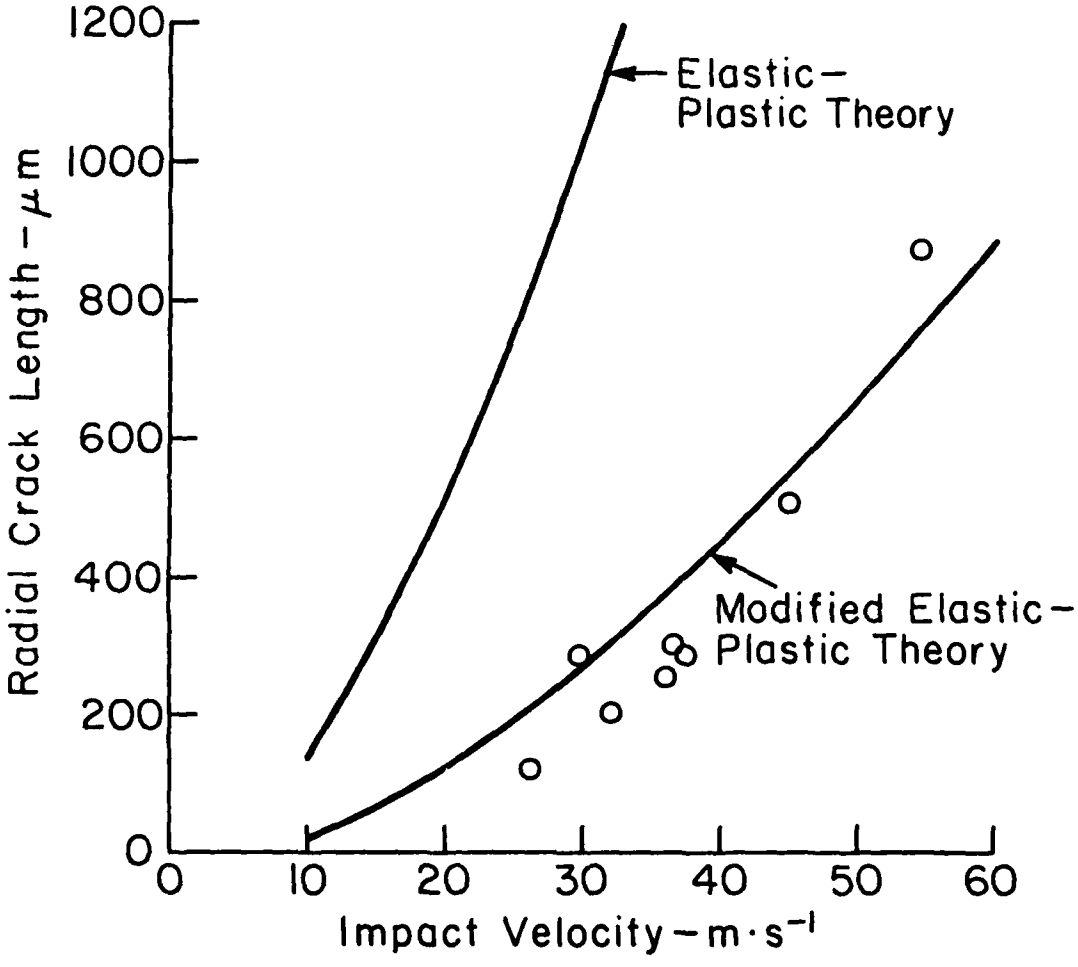

Figure [illegible] Radial crack length vs. impact velocity for the elastic-plastic theory and the modified elastic-elastic theory based on equations (10) and (11). (As-fired, TP-ZrO_2; 1.59 mm diameter tungsten carbide spheres).

VI. Summary and Discussion

The analysis developed in this program represents an attempt to obtain a general, self consistent means to calculate a wide range of impact characteristics using easily measured contact characteristics obtained under static loading conditions. Empirical equations are used to relate the contact and indentation pressures to the normalized contact and indentation radii. These empirical equations are manipulated using Newtonian mechanics, Hertzian elasticity and fracture mechanics methods to obtain equations for the contact radius, indentation radius, load, penetration time, crack size, remaining strength, contact time, and coefficient of restitution.

The comparisons of the theoretical calculations and experimental data presented in this report show that the results of the analysis can be used to make reasonable predictions of the response of a variety of ceramic materials to low velocity impact by spheres. On the whole, the results were improved by substitution of κ' for κ in the various equations to obtain the so-called modified elastic-plastic theory. Further evidence of the applicability of the relation $P/z_o \propto c^{1/2}$ to the localized impact damage case was presented. The exact form of the relation can have an important effect on the results when crack lengths are predicted by extrapolation to higher velocities where the commonly used $P \propto c^{3/2}$ relation tends to underestimate the crack length.

The fractographic investigation reported recently[8] and the present report have revealed a number of cases in which the present mathematical

model fails to provide a completely satisfactory representation of the impact phenomena:

1. The extent of plastic deformation seems to depend on the strain rate dependence of the flow stress. Therefore, the contact characteristics determined by static indentation provide only an approximate representation of the plastic deformation occurring during impact. The differences in extent of plastic deformation have important effects in the partitioning of energy among the various energy loss mechanisms, and the absolute and relative sizes of the various types of cracks.

2. The analysis neglects the stress wave energy and the fracture energy contributions to the energy balance. Although Hutchings[24] has determined that the stress wave energy makes only a minor contribution to the energy losses during impacts in which plastic deformation occurs, it is a fact that the above-mentioned strain rate dependence of the flow stress favors responses that are more elastic than otherwise expected and, in these cases, because the overall losses are lower, the stress wave energy is proportionately more important. Kirchner and Gruver[5] showed previously that the fracture surface energy makes a negligible contribution to the energy losses for low velocity impacts of glass spheres on glass plates. However, at higher velocities crushing occurs at the impact site and there is a substantial reduction in the coefficient of restitution indicating a substantial increase in energy losses. Under these conditions, little is known about the proportioning of the energy among the indentation, stress wave, friction, and fracture energy loss mechanisms.

3. Marshall and Lawn[25] have shown that residual stresses induced during static indentations have a substantial influence on the extent of crack propagation and remaining strength of glass. Kirchner and Isaacson[20] have shown that residual stresses

induced during single point machining of silicon nitride ceramics have similar effects. It is reasonable to expect that residual stresses are induced during localized impact but the effects of these stresses are not accounted for in the analysis.

4. The differences in K_{Ic} induced by aging treatments in TT-ZrO_2 do not result in the approximately two to one differences in crack size expected based on the present analysis. Failure to observe these differences may occur because the increased numbers of cracks induced in the lower K_{Ic} materials may act to reduce the K_I at the tips of these cracks, thus reducing the crack propagation below that otherwise expected. This observation confirms an earlier similar observation and may be important because increasing the K_{Ic} has been recommended by several investigators as a means to improve the resistance to localized impact damage.

Because the important role of the strain rate dependence of the flow stress is not accounted for in the contact characteristics, κ, κ', ξ, and ξ', determined by static loading, it is highly important to develop a method of determining the contact characteristics by impact tests. The present investigation indicates that the theoretical calculations of the coefficient of restitution are very sensitive to the κ to κ' ratio. Therefore, it seems reasonable to attempt to determine the contact characteristics by fitting the theoretical curves to the coefficient of restitution data. This procedure would also account for the stress wave and fracture energy losses. Development of this suggested method of determining the contact characteristics is recommended. The results can be evaluated based on the self consistency of the calculated values of the other impact characteristics.

Acknowledgements

The writers are pleased to acknowledge the contributions of R. C. Garvie and his associates at CSIRO who supplied the TT-ZrO_2 together with basic data on the material, D. M. Richard who developed the elastic-plastic impact theory, J. C. Conway, who derived the crack size equation, and their associates at Ceramic Finishing Company.

References

1. D. M. Richard and H. P. Kirchner, "Theory of Elastic-Plastic Impact on Ceramics," Proc. Fifth International Conference on Erosion by Liquid and Solid Impact, Cavendish Laboratory, U. of Cambridge (September, 1979) pages 27-1 to 27-10.

2. H. P. Kirchner and R. M. Gruver, "Localized Impact Damage in Glass," Mater. Sci. and Eng. 28, 153-160 (1977).

3. H. P. Kirchner and R. M. Gruver, "Branching of Hertz Cracks," in Fracture 1977, Vol. 3, Edited by D. M. R. Taplin, University of Waterloo Press, Waterloo, Ontario (1977), p. 959-964.

4. H. P. Kirchner and R. M. Gruver, "Localized Impact Damage in Stressed Members," Mater. Sci. and Eng. 28, 249-255 (1977).

5. H. P. Kirchner and R. M. Gruver, "The Effect of Localized Damage on Energy Losses During Impact," Mater. Sci. Eng. 33 (1) 101-106 (1978).

6. H. P. Kirchner, "Analysis of Localized Impact Damage in Biaxially Stressed Glass Plates," J. Amer. Ceram. Soc. 61 (3-4) 161-163 (1978).

7. H. P. Kirchner and R. M. Gruver, "Localized Impact Damage in a Viscous Medium (Glass)," in Fracture Mechanics of Ceramics, Vol. 3, Edited by R. C. Bradt, D. P. H. Hasselman, and F. F. Lange, Plenum (1978), p. 365-377.

8. H. P. Kirchner, T. J. Larchuk, and J. M. Ragosta, "Localized Impact Damage in Ceramics," Ceramic Finishing Company Technical Report No. 8, Contract N00014-74-C-0241 (February, 1980).

9. H. P. Kirchner and T. J. Larchuk, "Radial Crack Propagation During Contact Fracture of Zinc Sulfide," Presented at the Annual Meeting, American Ceramic Society (April, 1980).

10. H. P. Kirchner, R. M. Gruver, D. M. Richard, and R. C. Garvie, "Localized Impact Damage in Transformation Toughened Zirconia," Mater. Sci. Eng., 40, 49-57 (1979).

11. H. P. Kirchner, R. M. Gruver, M. V. Swain, and R. C. Garvie, "Crack Propagation and Branching in Transformation Toughened Zirconia," Presented at the Fall Meeting, Basic Science Division, American Ceramic Society (October, 1979), Submitted for publication.

12. H. P. Kirchner and J. Seretsky, "Improving Impact Resistance (of Silicon Nitride and Silicon Carbide) by Energy Absorbing Surface Layers," Bull. Amer. Ceram. Soc. 54 (6) 591-592 (June, 1975).

13. R. M. Gruver and H. P. Kirchner, "Effect of Leached Surface Layers on Impact Damage and Remaining Strength of Silicon Nitride," J. Amer. Ceram. Soc. 59 (1-2) 85-86 (January-February, 1976).

14. H. P. Kirchner and R. M. Gruver, "Localized Impact Damage in Stressed Si_3N_4 and Al_2O_3," Mater. Sci. Eng. 34, 25-31 (1978).

15. A. G. Evans and T. R. Wilshaw, "Quasi-Static Solid Particle Damage in Brittle Solids, I. Observations, Analysis and Implications," Acta. Met. 24, 939-956 (1976).

16. D. A. Schockey, K. C. Dao, and D. R. Curran, "Nucleation and Growth of Cracks in CVD ZnS Under Particle Impact, SRI Annual Report, Part II, Contract N00014-76-C-0657 (April, 1979), page 25.

17. S. Timoshenko and J. N. Goodier, "Theory of Elasticity," McGraw-Hill New York (1951).

18. F. C. Roesler, "Brittle Fractures Near Equilibrium," Proc. Phys. Soc. B69, 981-992 (1956).

19. B. R. Lawn and E. R. Fuller, "Equilibrium Penny-like Cracks in Indentation Fracture," J. Mater. Sci. 10, 2016-2024 (1975).

20. B. R. Lawn and D. B. Marshall, "Contact Fracture Resistance of Physically and Chemically Tempered Glass Plates: A Theoretical Model," Phys. Chem. Glasses 18 (1) 7-18 (1977).

21. H. P. Kirchner, R. M. Gruver, and D. M. Richard, "Fragmentation and Damage Penetration During Abrasive Machining of Ceramics," from The Science of Ceramic Machining and Surface Finishing II, Edited by B. J. Hockey and R. W. Rice, NBS Special Publication 562 (October, 1979) pages 23-42.

22. J. C. Conway and H. P. Kirchner, "The Mechanics of Crack Initiation and Propagation Beneath a Moving Sharp Indenter," To be published in J. Mater. Sci.

23. M. V. Swain, "Crack Nucleation About Pointed Indentations in Glasses," J. Amer. Ceram. Soc. 62 (5-6) 318-319 (1979).

24. I. M. Hutchings, "Energy Absorbed by Elastic Waves During Plastic Impact," J. Phys. D: Applied Physics 12 (11) 1819-24 (November, 1979).

25. D. B. Marshall and B. R. Lawn, "Residual Stress Effects in Sharp Contact Cracking, Part I, Indentation Fracture Mechanics," J. Mater. Sci. 14, 2001-2012 (1974).

26. H. P. Kirchner and E. D. Isaacson, "Material Removal and Damage Penetration During Abrasive Machining of Ceramics," Ceramic Finishing Co., Third Quarterly Report, Contract DAR 78-18097 (December, 1979).

27. A. G. Evans, "Strength Degradation by Projectile Impacts," J. Amer. Ceram. Soc. 56 (8) 405-409 (August, 1973).

28. D. G. Rickerby and N. H. MacMillan, "Mechanisms of Solid Particle Erosion in Crystalline Materials," Proc. Fifth International Conference on Erosion by Solid and Liquid Impact, Cavendish Laboratory, Cambridge U. (September, 1979), p. 29-1 to 29-6.

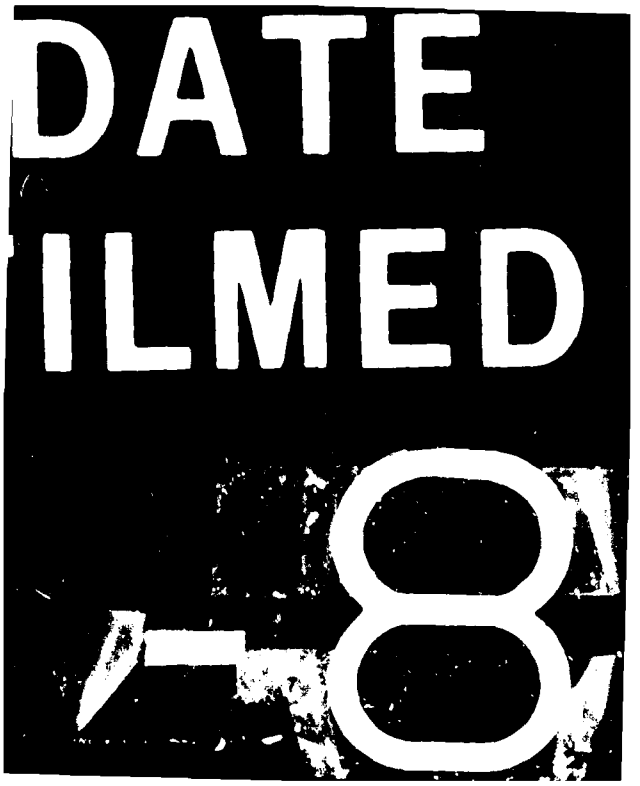
DATE
ILMED
8